Estimating atrial activity in epicardial electrograms

a beamforming perspective

by

Tijs Moree

to obtain the degree of Master of Science
at the Delft University of Technology,
to be defended publicly on Tuesday April 26th, 2022 at 10:15.

Student number:	4449479	
Project duration:	May 24, 2021 – April 26, 2022	
Thesis committee:	Dr. ir. Richard C. Hendriks,	TU Delft, supervisor
	Dr. ir. Daniele Cavallo,	TU Delft
	Drs. Mathijs S. van Schie,	Erasmus MC

An electronic version of this thesis is available at `http://repository.tudelft.nl/`.

TU Delft

Abstract

The most common serious heart rhythm disease is atrial fibrillation. It is not fatal on its own but does increase the risk of heart failures and strokes. There is little understanding about the mechanisms behind the disease, so more insight is desired. Using an array of electrodes, measurements are being performed of the electrical atrial activity directly on the heart tissue. These signals are, however, not clean and suffer from far-field interference coming from the ventricles.

During normal sinus rhythm these atrial and ventricular activities are separated in time and easy to distinguish. In case of atrial fibrillation this is not always the case. Luckily, there is a major difference between both signals: the ventricular signal comes from far away and arrives therefore approximately simultaneously at all electrodes. A simple, but effective way to remove this ventricular activity is to use a bipolar electrode. It produces the difference between two normal unipolar electrodes, thus removing the common ventricular signal component.

The bipolar electrode, however, distorts the atrial signal component, which in some orientations can even lead to removing it altogether. This bipolar electrode is known as a differential beamformer from the field of array signal processing. There are more complex beamformers that can keep the atrial component undistorted and therefore produce better results than the bipolar electrode.

This thesis proposes a Fourier-domain signal model for all available electrodes relying on an atrial and ventricular transfer function. It is possible to estimate these transfer functions from the data blindly. Three beamformers are derived utilizing the signal model and the transfer functions. The bipolar electrode is extended to multiple electrodes like the other beamformers as well.

Experiments with simulated data show that the complex beamformers indeed keep the atrial activity undistorted and are still able to remove the ventricular activity effectively when using multiple electrodes, except for very complex data where the signal model is not valid. For low numbers of electrodes the beamformers are not useful, they hardly remove the ventricular activity while keeping the atrial component undistorted, where the bipolar electrode does the opposite.

The electrograms are also used to estimate local activation times of the cells underneath the electrodes which says something about the health of the cardiac tissue. Besides the mentioned filtering, this thesis proposes a method to estimate those moments in time by looking at the time-domain version of the atrial transfer function, called the atrial impulse response. For simple data, it performs well compared to state-of-the-art methods, but for more complicated data, it does not.

Preface

From an early age, I knew I wanted to study in Delft with its big red and blue faculty you could see from the highway when passing by. All these years later, that very faculty has grown to be the decor of my student days. Now, after more than six and a half years, I am on the verge of finishing my studies and it has exceeded all expectations. The last year has been filled with reading, thinking, discussing, coding and writing, eventually resulting in the thesis you have in front of you right now.

This thesis explains my final project, which uses array signal processing to improve the readings, called electrograms, from an array of electrodes used to measure the electrical activity in the atria. This atrial activity is inspected to better understand a certain arrhythmia, atrial fibrillation. The electrograms suffer from far-field interference from the ventricles, which must be removed to enhance the data. The array signal processing technique, called beamforming, is used to first explain existing methods to filter the electrograms and then to improve them.

I started out in the bachelor of electrical engineering and ended up in the signal processing in the signals and systems track of the master of electrical engineering. Beamforming and other concepts used throughout the project can all be related back to those study years leading up to this last one. Besides these courses, however, I have other things and people to thank, for helping me achieve that masters' degree.

Acknowledgments

First, I would like to thank my supervisor Richard for helping me get through this project by asking questions, pushing me to think critically and reading the earlier versions of this thesis several times. Despite the biweekly meetings being mostly over zoom due to COVID-19, it has been very helpful to have a listening ear and receive the useful feedback.

I want to thank my parents and sister Loes for giving me all the opportunities to finally end up where I am now, for supporting me through my student career and for always being interested in what I was up to. You were a nice practice audience for explaining my thesis subject in *jip-en-janneketaal*.

I must also mention the Electrotechnische Vereeniging (ETV) for making my time at the TU Delft into the great years they were. I have spent countless hours on the couches in the Board room I could have used to speed up the studying, but there is no regret at all. Not only did I have a lot of fun and made friends for life, I also learned a great deal from the numerous activities, committees and the Board year in particular. The TU Delft gave me a powerful academic and technical background, but I owe my soft skills and further development to my days at the ETV.

Finally, I would like to thank my friends for all the fun distraction, the great vacations and for making my study days such a blast! I cannot imagine life without you guys.

Tijs Moree
Delft, April 2022

List of abbreviations

AA atrial activity

AF atrial fibrillation

AIR atrial impulse response

ARMSE atrial RMSE

ATF atrial transfer function

BE bipolar electrode

CC cross-correlation

CS covariance subtraction

CV conduction velocity

CVD cardiovascular disease

CW covariance whitening

DAS delay-and-sum

EBE extended bipolar electrode

ECG electrocardiogram

EGM epicardial electrogram

ETV Electrotechnische Vereeniging

EVD eigenvalue decomposition

FFT fast Fourier transform

GEVD generalized eigenvalue decomposition

IFFT inverse fast Fourier transform

LAT local activation time

LCMV Linear Constraint Minimum Variance

MVDR Minimum Variance Distortionless Response

RMSE root-mean-square error

SA sinoatrial node

SD steepest deflection

SNR signal-to-noise ratio

SR sinus rhythm

VA ventricular activity

VRMSE ventricular RMSE

VTF ventricular transfer function

Nomenclature

$(\cdot)^{\mathbf{H}}$ conjugate transpose operator

$*$ temporal convolution operator

F_s sampling frequency

M amount of sensor channels

$N_m[t]$ stochastic process of the noise component of an EGM

$S_{a,m}[t]$ stochastic process of the atrial component of an EGM

$S_{v,m}[t]$ stochastic process of the ventricular component of an EGM

$X_m[t]$ stochastic process of an EGM

$\delta[t]$ Dirac delta function

$\mathbf{1}$ all-ones vector of appropriate size

$\mathbf{I}$ identity matrix of appropriate size

$\mathbf{J}$ all-ones matrix of appropriate size

$\mathbf{R_A}$ atrial cross-correlation matrix

$\mathbf{R_N}$ noise cross-correlation matrix

$\mathbf{R_V}$ ventricular cross-correlation matrix

$\mathbf{R_X}$ noisy cross-correlation matrix

$\mathbf{R_{V+N}}$ interference cross-correlation matrix, consisting of the ventricular and noise components

$\mathbf{W}$ beamformer weights matrix

$\mathbf{a}$ atrial transfer function

$\mathbf{e}_i$ unit vector of appropriate size, where the ith entry is 1 and all others are 0

$\mathbf{n}$ realization of noise components of M EGMs in the frequency domain

$\mathbf{v}$ ventricular transfer function

$\mathbf{x}$ realization of M EGMs in the frequency domain

$\mathcal{F}\{\cdot\}$ Fourier transform operator

$\mathcal{F}^{-1}\{\cdot\}$ inverse Fourier transform operator

σ_a^2 variance of stochastic process $S_{a,m}[t]$

σ_n^2 variance of stochastic process $N_m[t]$

σ_v^2 variance of stochastic process $S_{v,m}[t]$

$\mathbf{E}[\cdot]$ expected value operator

f frequency bin

k time frame index

m electrode index

s_a common atrial signal component in all EGMs

s_v common ventricular signal component in all EGMs

t discrete time index

Contents

1 Introduction

Cardiovascular diseases (CVDs) are globally the biggest cause of death [1]. From the CVDs, the most common serious cardiac arrhythmia is atrial fibrillation (AF). It is not fatal on its own, but does increase the risk of heart failures and strokes and affects 1–2% of the population [2]. In the longer term almost 4% of middle aged men and women will have an incident hospitalization associated with AF and this number is likely to go up in the future.

This chapter introduces the basic concepts of this thesis. Section 1.1 gives an overview of the human heart and Section 1.2 explains AF. Section 1.3 gives insight in the way atrial activity (AA) is measured. Finally, Section 1.4 states the thesis objective and gives an overview of the rest of the thesis.

1.1. Anatomy

AF is an anomaly in the atria. To better understand the problem, we first describe the anatomy of the heart and its conduction system.

1.1.1. Human heart

The human heart makes sure blood circulates through the body. The blood then supplies the organs with oxygen and nutrients and removes carbon dioxide and other waste products. An image of the human heart and its main components is shown in Fig. 1.1. The heart has four chambers: two ventricles and two atria. The ventricles are the two biggest and lower situated chambers and the atria are the two small chambers on top. There are two sets of chambers for the two blood circulation routes as the lungs have a separate circulation.

When entering the heart from the hollow veins, the deoxygenated blood first flows into the right atrium, which contracts with a regular pulse and pushes the blood into the right ventricle, where the pulse continues, pumping the blood via the pulmonary artery into the lungs. There the gas exchange occurs: its oxygen level rises and its carbon-dioxide level drops. The blood flows via the pulmonary vein to the left side of the heart where it starts in the left atrium and continues in the left ventricle. The latter pumps the newly oxygenated blood into the aorta towards all other organs.

1.1.2. Cardiac conduction system

The contraction of the atrial and ventricular muscles happens under normal circumstances in a regulated fashion. A lump of pacemaking cells located in the wall of the right atrium and called the sinoatrial node (SA), determines and generates a pulse in the form of an electrochemical signal. The signal propagates in the form of cells being depolarized by their neighbors, conducting an excitation wave with a certain conduction velocity (CV). The cells remain depolarized for a little while, such that they can not be activated immediately again. This mechanism makes sure the wave does not propagate backwards. The moment of depolarization is called the local activation time (LAT).

The wave, starting in the SA node, travels through the right atrial muscle cells and via Bachman's bundle through the left atrial muscle cells as well. It spreads throughout the atria and makes them contract at once. After contraction of the atria, the signal gets delayed in the atrioventricular node

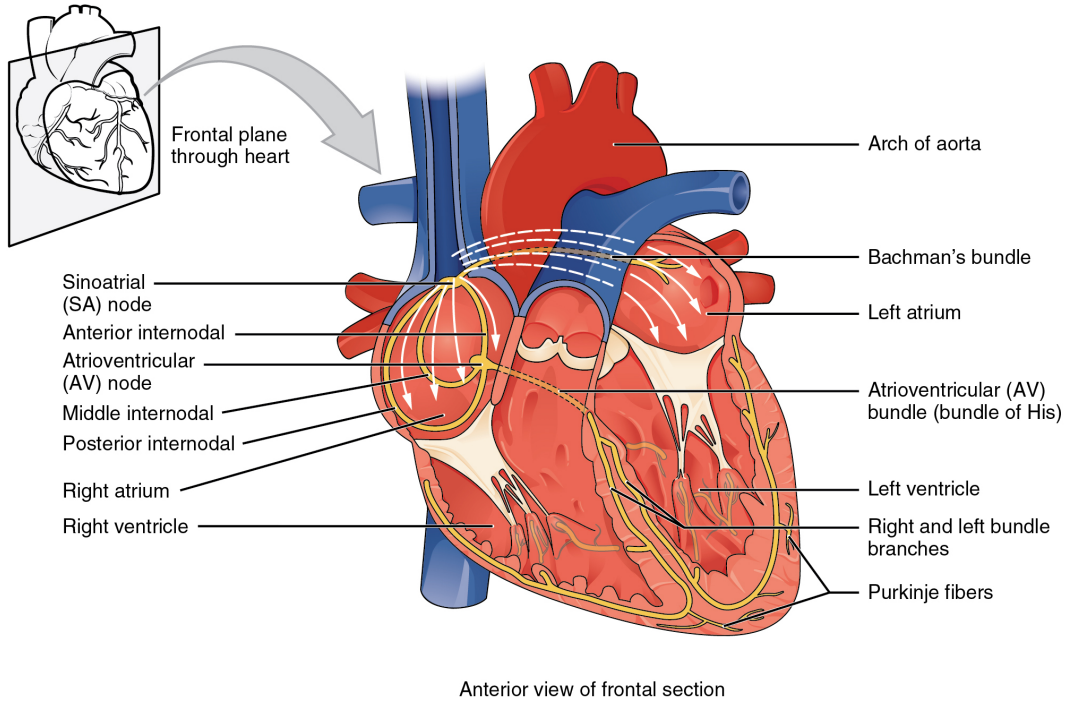

Figure 1.1: A schematic overview of the human heart with a highlighted conduction system [3].

to allow the blood to enter the ventricles. It continues to propagate through the bundle of His to the ventricles which contract at the same time as well.

1.2. Atrial fibrillation

In a healthy situation the rhythm at which the electrochemical signal propagates through the atria is called sinus rhythm (SR). In case of fibrillation, this rhythm however is not as regular as during SR. Atrial fibrillation is often described as a rapid, irregular and unsynchronized contraction of the atrial muscles. In case of ventricular fibrillation, the ventricles are not able to pump the blood through the body. The patient requires immediate medical treatment to prevent sudden cardiac death.

This thesis, however, concerns with the atria, in which case the effects of fibrillation are not as critical, albeit still unhealthy. AF is a disruption of the normal SR, causing an arrhythmic contraction of the atrial muscles. This reduces the power of the blood flow into the ventricles, resulting in higher risks of other heart problems in the long run.

1.2.1. Mechanisms

There is no general consensus on the mechanisms behind AF. However, there are several theories. One of the first was composed by Moe *et al.* who proposed that AF occurs due to the presence of multiple wavelets propagating through the atria [4]. These random wavelets of activation coexist and together generate an unorganized atrial rhythm. Another more recent theory states that AF is caused by so-called focal sources [5]. Random impulses deeper down in the heart tissue break through to the surface, generating a new activation wavefront. The last hypothesis proposes electrical rotors: activation waves propagating in a circular manner reexciting tissue [6].

1.2.2. Treatment

The most popular treatment of AF is catheter ablation. The process consists of a catheter being inserted into the body and navigated via the veins to the atria, where it ablates interfering tissue by making it either hot or cold, depending on the exact technique. The success rate is roughly 75% after multiple procedures [7]. The rate is way lower after running just a single procedure.

For treating a disease successfully, it is of paramount importance to have an understanding of the

mechanisms behind it. In the case of AF there is no general consensus regarding this necessary prerequisite for the treatment, hindering the development of a more successful treatment.

1.3. Measurements

To gain a better understanding of the origin of AF, it is important to do measurements and investigate the data. Historically, the heart rhythm is measured using electrodes on the skin, resulting in an electrocardiogram (ECG). This, however, is not detailed enough to say anything about the AA. The activity is therefore being measured during open-heart surgery using an array of electrodes placed directly on the atrial heart tissue. The data resulting from these electrodes is called an epicardial electrogram (EGM).

1.3.1. Interpretation

The EGMs were traditionally interpreted directly by cardiac physiologists as color-coded peak-to-peak voltage maps. Lower values would indicate an unhealthy area. Another approach is to determine the LAT of the cells underneath each electrode. These LATs would then be interpreted directly, or used to make a map of the CVs, which could once again be interpreted by a physiologist [8].

The EGMs, however, suffer from interfering ventricular activity (VA), caused by the depolarization of the ventricles. This big interfering signal distorts the pure AA and complicates further analysis and interpretation. This means, a method has to be found to remove the VA. Although, AA and VA may simply be separated in time in normal SR, this might not be the case in more complex situations like AF.

1.3.2. Types of electrodes

One method to remove VA has been applied in a hardware manner already. Most of the EGMs are measured using so-called unipolar electrodes. This means the voltages of all electrodes are measured against one common ground elsewhere on the body. This will result in the most pure AA, because the electrodes directly measure the polarizing and depolarizing cells underneath them. The unipolar electrode will, however, also pick up the the far-field VA.

This far-field component reaches the electrodes all approximately at the same time. Subtracting two closely located unipolar electrodes would therefore result in completely removing them. That is precisely what the bipolar electrode does. Synthesizing bipolar data from unipolar data is possible by considering the differences between two close unipolar electrodes, halving the amount of final electrode channels.

The method, however, comes with a lot of disadvantages. The VA will thus be suppressed in bipolar electrodes, but the AA will be affected as well. The literature shows that rotating a bipolar electrode has a big influence on its output as well as the direction of the atrial wave [9][10]. Both show using *in vivo* data that a wave front oblique to the electrode configuration is completely nullified.

Deno *et al.* have proposed a method to create a so-called omnidirectional electrode using two or three differently oriented closely located bipolar electrodes to overcome the direction dependency [11] [12]. Haldar *et al.* and Riccio *et al.* put the omnidirectional electrode to the test, comparing them to horizontal and vertical bipolar electrodes. Haldar confirms its independence of direction and its ability to determine the correct wave front direction [13]. Riccio comes to the same conclusion that the configuration indeed produces better and more consistent results regarding the direction of the wave front [14]. The omnidirectional electrode, however, feels like a naive solution from an array signal processing perspective. The literature just has not been able to explain the underlying problem. Looking at the set-up from a signal processing background will shed some light.

1.4. Thesis overview

The main goal of this thesis will be to apply the knowledge of signal processing to the problem of removing the VA in EGMs and with that making an estimate of the actual AA, such that further interpretation should be easier and more effective.

1.4.1. Objectives

The concept of beamforming in the Fourier domain will be applied to the EGMs, making use of the spatial correlation between all electrodes and using the simple fact that the interfering VA will reach all electrodes simultaneously. This will involve making estimates of so-called transfer function vectors and cross-correlation matrices.

The cleaned EGMs could then be used to make an estimate of the LATs using existing time domain methods. It is, however, also possible to make an estimate of those LATs directly from the aforementioned transfer function vectors. This will be the secondary goal of the thesis.

1.4.2. Overview

The thesis is divided into chapters. The signal model used throughout the thesis is described in Chapter 2, as well as the techniques used to estimate the transfer function vectors and cross-correlation matrices blindly from the EGM data. Chapter 3 uses the signal model to filter the EGMs in such a way that the VA is removed and the AA remains, applying beamformers in the Fourier domain. It describes the technique, implementation and results. Chapter 4 describes the estimation of the aforementioned LATs using that same signal model. It also contains the method, implementation and results. The results of both techniques are discussed in Chapter 5, as well as an overview of possible future work.

2

Signal model

In this chapter the signal model is described, that will be used throughout this thesis. It models the signals measured by an array of electrodes, placed directly on the atrial tissue, also called an EGM.

The signal model itself is proposed in Section 2.1 and the mathematics behind the estimation of the transfer functions are explained in Section 2.2.

2.1. Signal model

The EGMs are a filtered version of the action potentials inside the polarizing and depolarizing cells below the electrodes. The action potentials arise due to ion processes inside those cells and are therefore stochastic. The electrodes measure a weighted average of several underlying cell potentials. We assume that these averages will resemble a lot across the electrodes.

Besides this AA, the electrode will also pick up the VA, coming from the further away located ventricles. The remaining component in the EGM then is some self-noise of the sensor. These three signal components additively form an EGM. The signals are sampled with some sampling frequency F_s. Let m denote the electrode index and t the time sample index. The stochastic EGM $X_m[t]$ is then modeled as

$$X_m[t] = S_{a,m}[t] + S_{v,m}[t] + N_m[t], \tag{2.1}$$

where $S_{a,m}[t]$ and $S_{v,m}[t]$ are thus stochastic processes of the atrial and ventricular signal components respectively and $N_m[t]$ is the remaining stochastic noise process. The processes $S_{a,m}[t]$, $S_{v,m}[t]$ and $N_m[t]$ are assumed to be mutually independent.

The noise is considered to be a zero-mean white Gaussian process, where white means it has equal power across the frequency bands and Gaussian means it follows a normal distribution

$$N_m[t] \sim \mathcal{N}(0, \sigma_n^2). \tag{2.2}$$

A realization of process $X_m[t]$ will look like

$$x_m[t] = s_{a,m}[t] + s_{v,m}[t] + n_m[t], \tag{2.3}$$

where $x_m[t]$ is the measured signal, $s_{a,m}[t]$ and $s_{v,m}[t]$ are the atrial and ventricular signals respectively and $n_m[t]$ is the remaining noise. The model is described per time sample t and per sensor channel m of which there are M in total.

We assume that the propagation of the electric cardiac wave front can be modeled as a convolutive process between the stochastic atrial and ventricular sources $s_a[t]$ and $s_v[t]$ and the corresponding atrial and ventricular impulse responses $a_m[t]$ and $v_m[t]$ respectively. That is,

$$x_m[t] = \underbrace{(s_a * a_m)[t]}_{s_{a,m}[t]} + \underbrace{(s_v * v_m)[t]}_{s_{v,m}[t]} + n_m[t], \tag{2.4}$$

where the $*$ operator indicates a temporal convolution. An important notion to make here is that the sources $s_a[t]$ and $s_v[t]$ do not depend on the channel m; they are the same for all M channels. The

impulse responses $a_m[t]$ and $v_m[t]$ model the delay and damping of the sources due to propagation and electrode-cell distance respectively; they therefore do depend on the channel m as the propagation time and electrode-cell distance will be different per sensor.

Transforming the system to the frequency domain using the discrete Fourier transform per time frame k simplifies the model as the convolutions turn into simple multiplications. This results in

$$x_m[f, k] = \mathcal{F}\{x_m[t, k]\} = s_a[f, k]a_m[f, k] + s_v[f, k]v_m[f, k] + n_m[f, k], \tag{2.5}$$

with frequency bin f, Fourier transform operator $\mathcal{F}\{\cdot\}$ and transfer functions a_m and v_m for the atrial and ventricular signal parts respectively. Signal sources $s_a[f, k]$ and $s_v[f, k]$ once again do not depend on channel m. Combining all M sensor channels together in vectors gives the following expression

$$\mathbf{x} = s_a\mathbf{a} + s_v\mathbf{v} + \mathbf{n}. \tag{2.6}$$

The frequency index and time frame index have been omitted for notational simplicity, because the frequency bins and time frames can be manipulated independently.

In reality, there may be several differently shaped action potentials in the cells below the electrodes, resulting in multiple stochastic atrial sources instead of the one s_a, especially in the case of AF. This would result in a sum of multiple atrial signal source and transfer function combinations. This signal model, however, will only consider one atrial source and transfer function, which is a valid assumption [15].

2.1.1. Transfer function

Atrial transfer function (ATF) $\mathbf{a}$ and ventricular transfer function (VTF) $\mathbf{v}$ relate to the aforementioned impulse responses as their Fourier transforms. A transfer function is a vector containing information on the path the signal traveled from the signal source location to the sensor locations.

It is also possible to work with relative transfer functions. Dividing the whole vector by one of its entries, e.g. its first entry, will give a relative transfer function which models the transfer with respect to the reference electrode. The relative transfer function thus gives the path differences per sensor with respect to the one measured at that reference electrode. In fact, usually the absolute transfer function regarding the signal origin is only available up to a scalar ambiguity. This scalar ambiguity means it actually is a relative transfer function, whose reference is unknown. The information regarding the differences between the channels is still there.

2.1.2. Correlation matrix

The relations between the channels can be explained using the so-called cross-correlation matrix. It is an $M \times M$ matrix describing the correlation between the channels, defined as

$$\mathbf{R}_\mathbf{X} = \mathrm{E}\left[\mathbf{X}\mathbf{X}^{\mathrm{H}}\right], \tag{2.7}$$

with $\mathrm{E}[\cdot]$ the expected value operator and $(\cdot)^{\mathrm{H}}$ the conjugate transpose operator. One thing to note here is that the cross-correlation matrix is Hermitian, that is $\mathbf{R}_\mathbf{X} = \mathbf{R}_\mathbf{X}^{\mathrm{H}}$.

$\mathbf{X}$ is the stochastic process of all M channels of the EGMs in the frequency domain, that produces realizations $\mathbf{x}$. It is composed as

$$\mathbf{X} = \mathbf{S}_a + \mathbf{S}_v + \mathbf{N}. \tag{2.8}$$

The noisy cross-correlation matrix $\mathbf{R}_\mathbf{X}$ can then be written as

$$\mathbf{R}_\mathbf{X} = \mathrm{E}\left[(\mathbf{S}_a + \mathbf{S}_v + \mathbf{N})(\mathbf{S}_a + \mathbf{S}_v + \mathbf{N})^{\mathrm{H}}\right], \tag{2.9}$$

where many terms can be removed, because the three components of $\mathbf{R}_\mathbf{X}$ are considered mutually uncorrelated, as mentioned before. This results in

$$\mathbf{R}_\mathbf{X} = \mathrm{E}\left[\mathbf{S}_a\mathbf{S}_a^{\mathrm{H}} + \mathbf{S}_v\mathbf{S}_v^{\mathrm{H}} + \mathbf{N}\mathbf{N}^{\mathrm{H}}\right] = \mathbf{R}_\mathbf{A} + \mathbf{R}_\mathbf{V} + \mathbf{R}_\mathbf{N}, \tag{2.10}$$

where $\mathbf{R}_\mathbf{A}$ and $\mathbf{R}_\mathbf{V}$ are the cross-correlation matrices of the atrial and ventricular signal components and $\mathbf{R}_\mathbf{N}$ is the noise cross-correlation matrix. All three are Hermitian matrices, just like noisy cross-correlation matrix $\mathbf{R}_\mathbf{X}$.

Cross-correlation matrices can also be interpreted as cross-power spectral density matrices. The diagonal elements in fact indicate the energy in the corresponding channels. If the channels do not correlate at all, the cross-correlation matrix will be a diagonal matrix, that is only entries on the main diagonal are non-zero. The noise cross-correlation matrix for example is assumed to be

$$\mathbf{R_N} = \sigma_n^2 \mathbf{I}, \tag{2.11}$$

with noise signal variance σ_n^2 and identity matrix $\mathbf{I}$. The atrial and ventricular signal correlation matrices will not be diagonal matrices, since the signals correlate a lot among the electrodes due to the similar signal shapes s_a and s_v respectively.

The atrial cross-correlation matrix can be calculated as

$$\mathbf{R_A} = \mathrm{E}\left[\mathbf{A}\mathbf{A}^{\mathrm{H}}\right] = \mathrm{E}\left[s_a \mathbf{a}\mathbf{a}^{\mathrm{H}} s_a^{\mathrm{H}}\right], \tag{2.12}$$

where the transfer function $\mathbf{a}$ can be moved outside the expected value operator as it is considered deterministic. The remaining signal multiplication is stochastic and can be called atrial signal variance σ_a^2, leading to

$$\mathbf{R_A} = \mathrm{E}\left[s_a^{\mathrm{H}} s_a\right] \mathbf{a}\mathbf{a}^{\mathrm{H}} = \sigma_a^2 \mathbf{a}\mathbf{a}^{\mathrm{H}}. \tag{2.13}$$

The atrial cross-correlation matrix now is a rank-1 matrix. This once again is the case because the assumption was made that there only is one atrial signal source. The same derivations can be done for the ventricular signal component, resulting in

$$\mathbf{R_V} = \sigma_v^2 \mathbf{v}\mathbf{v}^{\mathrm{H}}. \tag{2.14}$$

The whole noisy cross-correlation matrix then looks like

$$\mathbf{R_X} = \sigma_a^2 \mathbf{a}\mathbf{a}^{\mathrm{H}} + \sigma_v^2 \mathbf{v}\mathbf{v}^{\mathrm{H}} + \sigma_n^2 \mathbf{I}, \tag{2.15}$$

where the last two terms together form the interference cross-correlation matrix $\mathbf{R_{V+N}}$, because the eventual goal is to remove the ventricular signal and noise components.

2.2. Transfer function estimation

In the following two chapters, the transfer functions and cross-correlation matrices play a big role and are assumed to be known. Determining the transfer functions, however, requires a very thorough understanding of the atrial tissue and the locations of the source and sensors, which in general is almost impossible. Furthermore, in the atrial problem, the tissue is precisely what is unknown.

An alternative for determining an expression for transfer functions is to make a blind estimate from the data itself by looking at the eigenvalue decomposition (EVD) [16] and generalized eigenvalue decomposition (GEVD) [17] of the noisy cross-correlation matrix $\mathbf{R_X}$.

2.2.1. Eigenvalue decomposition

The EVD is a way of factorizing a matrix into a standardized way where it is represented in terms of its eigenvalues and eigenvectors. An eigenvector $\mathbf{u}_i$ of a generic $M \times M$ matrix $\mathbf{A}$ is a normalized vector that only changes by a scalar factor when that matrix $\mathbf{A}$ is applied to it. That scalar factor then is the eigenvalue λ_i. This means

$$\mathbf{A}\mathbf{u}_i = \lambda_i \mathbf{u}_i. \tag{2.16}$$

Taking all M eigenvectors and eigenvalues together results in the following expression

$$\mathbf{A}\mathbf{U} = \mathbf{U}\mathbf{\Lambda}, \tag{2.17}$$

where $\mathbf{U}$ contain the eigenvectors $\mathbf{u}_i$ as columns and where $\mathbf{\Lambda}$ is a diagonal matrix containing the eigenvalues λ_i. These eigenvectors are called the right eigenvectors. We can also talk about left eigenvectors, that is

$$\mathbf{Q}^{\mathrm{H}}\mathbf{A} = \mathbf{\Lambda}\mathbf{Q}^{\mathrm{H}}, \tag{2.18}$$

where the left eigenvectors are the columns of $\mathbf{Q}$. The eigenvalues are not direction-dependent, which follows from rewriting Eq. (2.17) into

$$\mathbf{U}^{-1}\mathbf{A} = \mathbf{\Lambda}\mathbf{U}^{-1}, \tag{2.19}$$

which can be compared with Eq. (2.18). The left and right eigenvalues are thus the same. Also the following relation between left and right eigenvectors follows from the comparison

$$\mathbf{Q} = \mathbf{U}^{-\mathrm{H}}. \tag{2.20}$$

If $\mathbf{A}$ is a Hermitian matrix like the cross-correlation matrices are, the left and right eigenvectors are even the same, which follows from taking the Hermitian of both sides of Eq. (2.17)

$$\mathbf{U}^{\mathrm{H}}\mathbf{A}^{\mathrm{H}} = \mathbf{\Lambda}\mathbf{U}^{\mathrm{H}}, \tag{2.21}$$

and comparing this with Eq. (2.18).

2.2.2. Generalized eigenvalue decomposition

The GEVD is a generalization of the EVD with an extra $M \times M$ matrix $\mathbf{B}$. The GEVD is thus applied to a matrix pencil ($\mathbf{A}$, $\mathbf{B}$) such that

$$\mathbf{AU} = \mathbf{BU}\mathbf{\Lambda}, \tag{2.22}$$

and for the left GEVD

$$\mathbf{Q}^{\mathrm{H}}\mathbf{A} = \mathbf{\Lambda}\mathbf{Q}^{\mathrm{H}}\mathbf{B}. \tag{2.23}$$

The normal EVD is thus obtained by choosing the identity matrix for the secondary matrix $\mathbf{B} = \mathbf{I}$. If both $\mathbf{A}$ and $\mathbf{B}$ are Hermitian, the left and right generalized eigenvectors are the same, that is $\mathbf{U} = \mathbf{Q}$.

The GEVD can be rewritten into a normal EVD by considering the inverse of $\mathbf{B}$, that is

$$\mathbf{B}^{-1}\mathbf{AU} = \mathbf{U}\mathbf{\Lambda}, \tag{2.24}$$

for the right GEVD and

$$\mathbf{Q}^{\mathrm{H}}\mathbf{A}\mathbf{B}^{-1} = \mathbf{\Lambda}\mathbf{Q}^{\mathrm{H}}, \tag{2.25}$$

for the left case. These two equations show that the right generalized eigenvectors of ($\mathbf{A}$, $\mathbf{B}$) can also be obtained as the right normal eigenvectors of $\mathbf{B}^{-1}\mathbf{A}$ and the left generalized eigenvectors as the left normal eigenvectors of $\mathbf{A}\mathbf{B}^{-1}$.

2.2.3. Ventricular transfer function

The EVD and GEVD can be used to estimate the ATF and VTF. An important observation to make first from the problem is the difference between those transfer functions. The atrial signal component propagates through the tissue below the sensors, so there will be a lot of phase differences in the ATF, expressing the time delays between the moment the atrial wave activates the tissue under the electrodes.

The ventricular component, however, originates from relatively far away, meaning the phase differences inside the VTF are negligible and the magnitude differences are small. The VTF will therefore approximately be a normalized all-ones vector

$$\mathbf{v} \approx \frac{1}{\sqrt{M}}\mathbf{1}. \tag{2.26}$$

We could also try to make a better estimate of $\mathbf{v}$ by looking at the eigenvectors of $\mathbf{R}_{\mathbf{X}}$ and selecting the one closest to the all-ones vector. The EVD of $\mathbf{R}_{\mathbf{X}}$ is composed as

$$\mathbf{R}_{\mathbf{X}}\mathbf{U} = \mathbf{U}\mathbf{\Lambda}. \tag{2.27}$$

Because $\mathbf{R}_{\mathbf{X}}$ is Hermitian, $\mathbf{U}$ is a unitary matrix, that is $\mathbf{U}^{-1} = \mathbf{U}^{\mathrm{H}}$. This results in

$$\mathbf{R}_{\mathbf{X}} = \mathbf{U}\mathbf{\Lambda}\mathbf{U}^{\mathrm{H}}. \tag{2.28}$$

From the comparison of this equation with Eq. (2.15), we make the assumption that one of the columns of $\mathbf{U}$ corresponds with the VTF and therefore resembles the all-ones vector. This resemblance can be measured by looking at the dot-product of each eigenvector with the all-ones vector. The best estimate of the VTF can then be selected by maximizing that dot product, which comes down to

$$\hat{\mathbf{v}} = \arg\max \mathbf{U}^{\mathrm{H}}\mathbf{1}. \tag{2.29}$$

Because the eigenvectors are normalized vectors and the estimate of the VTF is one of those eigenvectors, we can say that the VTF is normalized as well, resulting in $\mathbf{v}^{\mathrm{H}}\mathbf{v} = 1$. Furthermore, due to the lack of phase differences among this VTF, it is actually possible to enhance the estimate by averaging it across frequency bins f. This should remove any deviations and result in a better estimate than the simple all-ones vector. The resulting estimate of the VTF then still is approximately normalized.

The interference cross-correlation matrix then is fully describable as

$$\mathbf{R}_{\mathbf{V+N}} = \sigma_v^2 \mathbf{v}\mathbf{v}^{\mathrm{H}} + \sigma_n^2 \mathbf{I}. \tag{2.30}$$

The missing information in this expression is the mixing of these two matrices, which depends on the signal powers. The ventricular signal power is generally larger than the noise signal power. For now the mixing constant is assumed to be known, but generally, $\sigma_v^2 \gg \sigma_n^2$.

2.2.4. Atrial transfer function

With this general knowledge of the interference, it is possible to get an idea of the atrial cross-correlation matrix $\mathbf{R}_{\mathbf{A}}$. There are generally two ways of going about this. The first one is covariance subtraction (CS), which simply subtracts the interference cross-correlation matrix from the noisy one to come to an expression of the atrial one. This, however, has proven to give unstable results [18].

The other option is covariance whitening (CW), using the interference cross-correlation matrix $\mathbf{R}_{\mathbf{V+N}}$ to "pre-whiten" the noisy cross-correlation matrix $\mathbf{R}_{\mathbf{X}}$. Pre-whitening means turning the interference present in the noisy cross-correlation matrix into white noise. Then afterwards, the noise cross-correlation matrix can be considered to be a simple identity matrix, which simplifies a lot of following computation steps.

Pre-whitening can be done by comparing the GEVDs of matrix pencils $(\mathbf{R}_{\mathbf{X}}, \mathbf{R}_{\mathbf{V+N}})$ and $(\mathbf{R}_{\mathbf{A}}, \mathbf{R}_{\mathbf{V+N}})$, where $\mathbf{R}_{\mathbf{X}}$ can be determined from the data itself, $\mathbf{R}_{\mathbf{V+N}}$ has been composed using several assumptions in the previous section and $\mathbf{R}_{\mathbf{A}}$ is to be determined. Starting with the decomposition of $(\mathbf{R}_{\mathbf{A}}, \mathbf{R}_{\mathbf{V+N}})$, a non-singular matrix $\mathbf{U}$ and diagonal matrix $\mathbf{\Lambda}$ can be found that conform to the following two equations

$$\mathbf{U}^{\mathrm{H}}\mathbf{R}_{\mathbf{A}}\mathbf{U} = \mathbf{\Lambda}, \tag{2.31}$$

and

$$\mathbf{U}^{\mathrm{H}}\mathbf{R}_{\mathbf{V+N}}\mathbf{U} = \mathbf{I}. \tag{2.32}$$

This decomposition of $\mathbf{R}_{\mathbf{A}}$ and $\mathbf{R}_{\mathbf{V+N}}$ into $\mathbf{U}$ and $\mathbf{\Lambda}$ is called the GEVD of matrix pencil $(\mathbf{R}_{\mathbf{A}}, \mathbf{R}_{\mathbf{V+N}})$, where $\mathbf{U}$ contains the generalized eigenvectors and $\mathbf{\Lambda}$ is a diagonal matrix containing the generalized eigenvalues. Without loss of generality, we assume the generalized eigenvalues are sorted from big to small. The two equations can be combined into the characteristic GEVD equation

$$\mathbf{R}_{\mathbf{A}}\mathbf{U} = \mathbf{R}_{\mathbf{V+N}}\mathbf{U}\mathbf{\Lambda}. \tag{2.33}$$

Rewriting Eqs. (2.31) and (2.32) using $\mathbf{Q} = \mathbf{U}^{-\mathrm{H}}$, gives

$$\mathbf{R}_{\mathbf{A}} = \mathbf{Q}\mathbf{\Lambda}\mathbf{Q}^{\mathrm{H}}, \tag{2.34}$$

and

$$\mathbf{R}_{\mathbf{V+N}} = \mathbf{Q}\mathbf{Q}^{\mathrm{H}}. \tag{2.35}$$

A sum of these equations gives

$$\mathbf{R}_{\mathbf{X}} = \mathbf{R}_{\mathbf{A}} + \mathbf{R}_{\mathbf{V+N}} = \mathbf{Q}\left(\mathbf{\Lambda} + \mathbf{I}\right)\mathbf{Q}^{\mathrm{H}}, \tag{2.36}$$

$$\mathbf{U}^{\mathrm{H}}\mathbf{R}_{\mathbf{X}}\mathbf{U} = \mathbf{\Lambda} + \mathbf{I}. \tag{2.37}$$

Comparing this equation with Eq. (2.31) shows that the GEVD of $(\mathbf{R}_{\mathbf{X}}, \mathbf{R}_{\mathbf{V+N}})$ will produce the same generalized eigenvectors as $(\mathbf{R}_{\mathbf{A}}, \mathbf{R}_{\mathbf{V+N}})$ and the same eigenvalues by subtracting unity.

Pre-whitening can thus be done using the GEVD, which results in an expression of the atrial cross-correlation matrix $\mathbf{R}_{\mathbf{A}}$. In reality, this matrix will not be calculated explicitly, because its decomposition can be used directly to get an expression of ATF $\mathbf{a}$. Comparing Eq. (2.34) with Eq. (2.13), shows that $\mathbf{\Lambda}$ contains one non-zero value, since $\mathbf{R}_{\mathbf{A}} = \sigma_a^2 \mathbf{a}\mathbf{a}^{\mathrm{H}}$ is a rank-1 matrix. This will be the first generalized

eigenvalue due to the sorting. The column of $\mathbf{Q}$ corresponding to this one non-zero value in $\mathbf{\Lambda}$ then is the ATF $\mathbf{a}$ with a scalar ambiguity, that is

$$\hat{\mathbf{a}} = \mathbf{Q}\mathbf{e}_1, \tag{2.38}$$

with $\mathbf{e}_i$ being the ith unit vector, meaning its ith entry is 1 and all others are 0. Once again, the ATF is a normalized vector, just like the VTF, because it is one of the eigenvectors. This means $\mathbf{a}^{\mathrm{H}}\mathbf{a} = 1$.

This $\mathbf{Q}$ can thus be calculated as the inverse Hermitian of matrix $\mathbf{U}$ which is obtained from the GEVD of pencil $(\mathbf{R}_{\mathbf{X}}, \mathbf{R}_{\mathbf{V+N}})$. These generalized eigenvectors can then also be derived as the normal eigenvectors of $\mathbf{R}_{\mathbf{V+N}}^{-1}\mathbf{R}_{\mathbf{X}}$. The normal left eigenvectors of that $\mathbf{R}_{\mathbf{V+N}}^{-1}\mathbf{R}_{\mathbf{X}}$ will then actually be that matrix $\mathbf{Q}$, since those normal left eigenvectors will relate to the normal right eigenvectors as $\mathbf{Q} = \mathbf{U}^{-\mathrm{H}}$.

3

Estimating atrial activity

In this chapter the signal model is used to filter the EGMs in such a way that the VA is removed and the AA remains with as little noise and interference as possible.

Some similar methods from the literature are discussed in Section 3.1. The method proposed in this thesis is explained in Section 3.2. A first theoretical analysis of this method is done in Section 3.3, the MATLAB implementation is explained in Section 3.4 and the results of the method can be seen in Section 3.5.

3.1. Literature

The literature, of course, already shows many algorithms with the same goal. The simplest option is separating the atrial and ventricular signals in time, but this is only possible when they do not overlap. The other solution mentioned in the introduction is the bipolar electrode, which removes the VA effectively, but also affects the AA. There are other more complex methods as well. Most were originally meant for use against ECGs, but can be used with EGMs as well. Below are the two main examples.

3.1.1. Template matching

One of the early methods in literature is template matching and subtraction [19] [20]. It uses a database of stereotypical ventricular signal components and matches those to new data to be able to cancel that signal component, leaving only the AA. It usually involves a corresponding ECG to know where to look for VA and is of low computation complexity. The problem, however, is that the subtraction leaves bad artifacts [21].

3.1.2. Blind source separation

The second method is blind source separation, which bases its technique on the assumption that AA and VA are decoupled, meaning they can be considered as originating from two different sources [22]. The method presented in this thesis actually relies on the same assumption. In blind source separation the different sources, that is the AA and VA, are distinguished using principle component analysis or independent component analysis methods [23] [24]. The method does, however, not result in a perfect estimation of the AA, because, in reality, the AA and VA are not fully decoupled.

3.2. Method

The method proposed in this thesis thus uses the assumption that the AA and VA come in from a different direction. Using the signal model presented in Chapter 2, it is possible to make a smart combination of that spatial information to remove signals from particular directions while preserving those coming in from other directions. This phenomenon is called beamforming [25].

3.2.1. State-of-the-art beamformers

Let us consider a simpler signal model to demonstrate several beamformers

$$\mathbf{x} = s\mathbf{d} + \mathbf{n}, \tag{3.1}$$

where s is the desired signal, $\mathbf{d}$ is its transfer function and $\mathbf{n}$ is noise that we want to remove as much as possible. A beamformer can then be considered a spatial filter denoted by a vector $\mathbf{w}$ containing the beamformer weights, used as

$$\hat{s} = \mathbf{w}^{\mathrm{H}}\mathbf{x} = s\mathbf{w}^{\mathrm{H}}\mathbf{d} + \mathbf{w}^{\mathrm{H}}\mathbf{n}. \tag{3.2}$$

By properly choosing $\mathbf{w}$, the beamformer will estimate the signal of interest at the reference electrode of transfer function $\mathbf{d}$.

One of the simplest examples is the delay-and-sum (DAS) beamformer [26]. In the time domain, it compensates for the delays of each channel for a certain incoming angle and sums those delayed signals. In the frequency domain this can be accomplished using the Hermitian of transfer function $\mathbf{d}$. The main benefit of using this technique over simply using one of the channels as estimate for the original signal is the averaging and therefore diminishing effect on the noise, assuming the noise is spatially uncorrelated. The signal itself will constructively interfere and will therefore not diminish. The beamformer expression is given by

$$\mathbf{w}_{\mathrm{DAS}} = \frac{\mathbf{d}}{\mathbf{d}^{\mathrm{H}}\mathbf{d}}, \tag{3.3}$$

and the resulting estimate is

$$\hat{s}_{\mathrm{DAS}} = s + \frac{\mathbf{d}^{\mathrm{H}}\mathbf{n}}{\mathbf{d}^{\mathrm{H}}\mathbf{d}}. \tag{3.4}$$

There is more to achieve in terms of noise cancellation by building more advanced beamformers. The Minimum Variance Distortionless Response (MVDR) beamformer, for example, aims to reduce the noise as much as possible, while still keeping the signal component s undistorted [27]. In the DAS beamformer the signal component was undistorted as well, but the MVDR is able to remove the noise more effectively by making use of the noise cross-correlation matrix. It is composed as a minimization problem, where the output power is being minimized under the constraint not to distort the target. This is the same as minimizing the output noise power under the same constraint, because the signal noise cannot be minimized due to that constraint. The noise output power can be calculated as

$$P_{n,\mathrm{out}} = \mathrm{E}\left[\left(\mathbf{w}^{\mathrm{H}}\mathbf{n}\right)\left(\mathbf{w}^{\mathrm{H}}\mathbf{n}\right)^{\mathrm{H}}\right] = \mathbf{w}^{\mathrm{H}}\mathbf{R}_{\mathbf{N}}\mathbf{w}. \tag{3.5}$$

The beamformer can then be derived from

$$\begin{aligned} \min_{\mathbf{w}^{\mathrm{H}}} \quad & \mathbf{w}^{\mathrm{H}}\mathbf{R}_{\mathbf{N}}\mathbf{w} \\ \text{s.t.} \quad & \mathbf{w}^{\mathrm{H}}\mathbf{d} = 1. \end{aligned} \tag{3.6}$$

This minimization problem is convex and can be solved using the lagrangian

$$L(\lambda) = \mathbf{w}^{\mathrm{H}}\mathbf{R}_{\mathbf{N}}\mathbf{w} + \lambda\left(\mathbf{w}^{\mathrm{H}}\mathbf{d} - 1\right). \tag{3.7}$$

Finding the minimum with respect to $\mathbf{w}^{\mathrm{H}}$ of this lagrangian results in

$$\mathbf{w}_{\mathrm{MVDR}} = \frac{\mathbf{R}_{\mathbf{N}}^{-1}\mathbf{d}}{\mathbf{d}^{\mathrm{H}}\mathbf{R}_{\mathbf{N}}^{-1}\mathbf{d}}. \tag{3.8}$$

The beamformer results in the following signal estimate

$$\hat{s}_{\mathrm{MVDR}} = s + \frac{\mathbf{d}^{\mathrm{H}}\mathbf{R}_{\mathbf{N}}^{-1}\mathbf{n}}{\mathbf{d}^{\mathrm{H}}\mathbf{R}_{\mathbf{N}}^{-1}\mathbf{d}}. \tag{3.9}$$

It is possible to introduce an extra constraint in the minimization problem to nullify a signal component besides the noise, coming in from a different direction explicitly, for example. A beamformer with multiple linear constraints is called a Linear Constraint Minimum Variance (LCMV), which is a generalization of the MVDR [27]. If we would like to remove a signal with transfer function $\mathbf{r}$, the beamformer can be composed as

$$\begin{aligned} \min_{\mathbf{w}^{\mathrm{H}}} \quad & \mathbf{w}^{\mathrm{H}}\mathbf{R}_{\mathbf{N}}\mathbf{w} \\ \text{s.t.} \quad & \mathbf{w}^{\mathrm{H}}\mathbf{d} = 1 \\ \text{s.t.} \quad & \mathbf{w}^{\mathrm{H}}\mathbf{r} = 0, \end{aligned} \tag{3.10}$$

which is a convex minimization problem, just like the MVDR formulation. It can again be solved using the lagrangian, that is

$$L(\lambda, \kappa) = \mathbf{w}^{\mathrm{H}}\mathbf{R_N}\mathbf{w} + \lambda\left(\mathbf{w}^{\mathrm{H}}\mathbf{d} - 1\right) + \kappa\left(\mathbf{w}^{\mathrm{H}}\mathbf{r}\right). \tag{3.11}$$

Minimizing with respect to $\mathbf{w}^{\mathrm{H}}$, results in the following beamformer

$$\mathbf{w}_{\mathrm{LCMV}} = \frac{\mathbf{R_N^{-1}}(\mathbf{r}^{\mathrm{H}}\mathbf{R_N^{-1}}\mathbf{r}\mathbf{d} - \mathbf{r}^{\mathrm{H}}\mathbf{R_N^{-1}}\mathbf{d}\mathbf{r})}{\mathbf{d}^{\mathrm{H}}\mathbf{R_N^{-1}}(\mathbf{r}^{\mathrm{H}}\mathbf{R_N^{-1}}\mathbf{r}\mathbf{d} - \mathbf{r}^{\mathrm{H}}\mathbf{R_N^{-1}}\mathbf{d}\mathbf{r})}. \tag{3.12}$$

3.2.2. Beamformer matrix

Beamformers focus on estimating the signal component s, which means all M channels are combined into one estimate $\hat{s}$. We are, however, interested in filtering all M channels. We can do so by multiplying the estimated $\hat{s}$ with transfer function $\mathbf{d}$ to get an estimate of the desired signal in each channel, that is,

$$\hat{\mathbf{s}} = \hat{s}\mathbf{d} = \left(\mathbf{w}^{\mathrm{H}}\mathbf{x}\right)\mathbf{d}, \tag{3.13}$$

which can also be done inside the beamformer by right-multiplying it with the Hermitian of the transfer function, turning it into a beamformer matrix $\mathbf{W}$, as follows from

$$\hat{\mathbf{s}} = \left(\mathbf{w}^{\mathrm{H}}\mathbf{x}\right)\mathbf{d} = \mathbf{d}\left(\mathbf{w}^{\mathrm{H}}\mathbf{x}\right) = \left(\mathbf{w}\mathbf{d}^{\mathrm{H}}\right)^{\mathrm{H}}\mathbf{x} = \mathbf{W}^{\mathrm{H}}\mathbf{x}. \tag{3.14}$$

For the DAS beamformer, this beamformer matrix looks like

$$\mathbf{W}_{\mathrm{DAS}} = \frac{\mathbf{d}\mathbf{d}^{\mathrm{H}}}{\mathbf{d}^{\mathrm{H}}\mathbf{d}}. \tag{3.15}$$

Multiplying this matrix with the measured signals $\mathbf{x}$ will thus give a filtered version of that signal of each channel instead of just at one channel.

3.2.3. Bipolar electrode as beamformer

The bipolar electrode (BE) mentioned in the introduction can also be placed in the context of beamformers. It actually is part of the class of differential beamformers [28]. In the time domain it consists of a simple subtraction between two close electrodes. To compare it with other beamformers, we will extend it from two to M electrodes by considering its effect as removing the mean across all channels from each channel, resulting in the extended bipolar electrode (EBE), that is,

$$\hat{s}_{a,m}[t] = x_m[t] - \frac{1}{M}\sum_m x_m[t], \tag{3.16}$$

which in case of $M = 2$ translates to

$$\hat{s}_{a,2}[t] = \frac{1}{2}\left(x_2[t] - x_1[t]\right), \tag{3.17}$$

which is the subtraction we recognize from the BE expression. To fully be able to compare it with other beamformers, we need to move it to the frequency domain. It does not require any delays, so there are no frequency-dependent factors, meaning the beamformer will be the same across all frequency bins, given by

$$\mathbf{W}_{\mathrm{EBE}} = \mathbf{I} - \frac{1}{M}\mathbf{J}, \tag{3.18}$$

where $\mathbf{J}$ is the all-ones matrix $\mathbf{J} = \mathbf{1}\mathbf{1}^{\mathrm{H}}$.

The subtraction of the mean of the signal is of course trying to remove the ventricular signal and actually assumes the ventricular signal is the same across all channels, meaning it assumes an all-ones VTF. We can make a slight adjustment to the beamformer so to turn the mean into a weighted average to be able to use a better estimate of the VTF than the simple all-ones vector. This looks like

$$\mathbf{W}_{\mathrm{EBE}} = \mathbf{I} - \frac{\mathbf{v}\mathbf{v}^{\mathrm{H}}}{\mathbf{v}^{\mathrm{H}}\mathbf{v}} = \mathbf{I} - \mathbf{v}\mathbf{v}^{\mathrm{H}}, \tag{3.19}$$

where $\mathbf{v}^{\mathrm{H}}\mathbf{v} = 1$, because $\mathbf{v}$ is an orthonormal eigenvector.

The right-hand side of the expression can now be interpreted as a DAS beamformer trying to estimate the ventricular signal component. The EBE can then be read as a filter that estimates the ventricular signal component using a DAS and subtracts that from signal $\mathbf{x}$.

3.2.4. Back to the signal model

Going back to the problem posed in this thesis, we can use beamformers to filter signal $\mathbf{x}$ such that the ventricular signal component $\mathbf{s}_v = s_v\mathbf{v}$ is removed while atrial signal component $\mathbf{s}_a = s_a\mathbf{a}$ is preserved. The placeholder transfer function $\mathbf{d}$ will therefore be the ATF $\mathbf{a}$ from now on. The transfer function $\mathbf{r}$ used in the LCMV expression will be the VTF $\mathbf{v}$. Furthermore, we need beamformer matrices, so the original beamformer expressions are extended with the Hermitian of the ATF from the right.

The expression for the DAS beamformer in Eq. (3.3) then results in

$$\mathbf{W}_{\text{DAS}} = \mathbf{a}\mathbf{a}^{\text{H}}, \tag{3.20}$$

where the original denominator could be simplified using the fact that $\mathbf{a}^{\text{H}}\mathbf{a} = 1$, as $\mathbf{a}$ was found as one of the orthonormal eigenvectors.

The state-of-the-art MVDR and LCMV beamformers, need some more changes to be applicable to the relevant signal model. The MVDR expression in Eq. (3.8) should not simply use the noise cross-correlation matrix $\mathbf{R_N}$, but should consider the ventricular component to be noise as well. It will therefore use the interference cross-correlation matrix $\mathbf{R_{V+N}}$. The MVDR actually uses the inverse of that matrix, which can be calculated using the Sherman–Morrison formula due to its special form using the ventricular rank-1 cross-correlation matrix [29]. The formula states that for generic matrix $\mathbf{A}$ and vectors $\mathbf{u}$ and $\mathbf{v}$ the following inverse holds,

$$\left(\mathbf{A} + \mathbf{u}\mathbf{v}^{\text{H}}\right)^{-1} = \mathbf{A}^{-1} - \frac{\mathbf{A}^{-1}\mathbf{u}\mathbf{v}^{\text{H}}\mathbf{A}^{-1}}{1 + \mathbf{v}^{\text{H}}\mathbf{A}^{-1}\mathbf{u}}. \tag{3.21}$$

This results in our case in,

$$\mathbf{R}_{\mathbf{V+N}}^{-1} = \left(\sigma_n^2\mathbf{I} + \sigma_v^2\mathbf{v}\mathbf{v}^{\text{H}}\right)^{-1} = \frac{1}{\sigma_n^2}\mathbf{I} - \frac{\sigma_v^2}{\sigma_n^2\left(\sigma_v^2 + \sigma_n^2\right)}\mathbf{v}\mathbf{v}^{\text{H}}. \tag{3.22}$$

Using this inverse, the MVDR applicable to the signal model can be rewritten into

$$\mathbf{W}_{\text{MVDR}} = \frac{\left(1 + \frac{\sigma_n^2}{\sigma_v^2}\right)\mathbf{a}\mathbf{a}^{\text{H}} - \left(\mathbf{v}^{\text{H}}\mathbf{a}\right)\mathbf{v}\mathbf{a}^{\text{H}}}{1 + \frac{\sigma_n^2}{\sigma_v^2} - \left(\mathbf{v}^{\text{H}}\mathbf{a}\right)\left(\mathbf{a}^{\text{H}}\mathbf{v}\right)}, \tag{3.23}$$

where a few simplifications were made using $\mathbf{a}^{\text{H}}\mathbf{a} = 1$ and $\mathbf{v}^{\text{H}}\mathbf{v} = 1$.

The LCMV expression in Eq. (3.12) does not need to use the $\mathbf{R_{V+N}}$, because the ventricular component is already explicitly set in the constraints. It will just use the noise cross-correlation matrix, which can be filled out, resulting in

$$\mathbf{W}_{\text{LCMV}} = \frac{\mathbf{a}\mathbf{a}^{\text{H}} - \left(\mathbf{v}^{\text{H}}\mathbf{a}\right)\mathbf{v}\mathbf{a}^{\text{H}}}{1 - \left(\mathbf{v}^{\text{H}}\mathbf{a}\right)\left(\mathbf{a}^{\text{H}}\mathbf{v}\right)}. \tag{3.24}$$

3.3. Analysis

The beamformers can be analyzed theoretically against the proposed signal model, showing whether they should have nice results for EGMs that exactly conform to the signal model. In reality, this will of course not be the case. The tests with simulated and real-life data will eventually have to show whether the assumptions are close enough to the truth. First, however, we test the proposed beamformers theoretically against the signal model, that is

$$\hat{\mathbf{s}}_a = \mathbf{W}^{\text{H}}\mathbf{x} = s_a\mathbf{W}^{\text{H}}\mathbf{a} + s_v\mathbf{W}^{\text{H}}\mathbf{v} + \mathbf{W}^{\text{H}}\mathbf{n}. \tag{3.25}$$

It follows that a good result would arise if the beamformer matrix $\mathbf{W}$ would adhere to $\mathbf{W}^{\text{H}}\mathbf{a} = \mathbf{a}$, $\mathbf{W}^{\text{H}}\mathbf{v} = \mathbf{0}$ and $\mathbf{W}^{\text{H}}\mathbf{n} = \mathbf{0}$. The first two objectives are easier to accomplish than the last one, because they only consist of deterministic terms, while the last one wants to cancel noise $\mathbf{n}$, which is stochastic. We only have indirect information on that noise and that last objective can therefore only be aimed for indirectly, like the MVDR does using the deterministic noise cross-correlation matrix $\mathbf{R_N}$. Luckily, the noise will generally be the smallest signal component, wherefore that last objective is the least important.

3.3.1. Theoretical results

Testing the EBE against the three objectives, shows that there is room for improvement. While the ventricular signal component is removed, which follows from

$$\mathbf{W}_{\mathrm{EBE}}^{\mathrm{H}}\mathbf{v} = \left(\mathbf{I} - \mathbf{v}\mathbf{v}^{\mathrm{H}}\right)^{\mathrm{H}}\mathbf{v} = \mathbf{v} - \left(\mathbf{v}^{\mathrm{H}}\mathbf{v}\right)\mathbf{v} = \mathbf{0}, \tag{3.26}$$

the atrial signal component is distorted,

$$\mathbf{W}_{\mathrm{EBE}}^{\mathrm{H}}\mathbf{a} = \left(\mathbf{I} - \mathbf{v}\mathbf{v}^{\mathrm{H}}\right)^{\mathrm{H}}\mathbf{a} = \mathbf{a} - \left(\mathbf{v}^{\mathrm{H}}\mathbf{a}\right)\mathbf{v} \neq \mathbf{a}. \tag{3.27}$$

Let us test the more complex beamformers, that actually all keep the atrial part undistorted and remove the ventricular in varying degrees. Starting with the DAS one from Eq. (3.20), whose ventricular signal component results in

$$\mathbf{W}_{\mathrm{DAS}}^{\mathrm{H}}\mathbf{v} = \left(\mathbf{a}\mathbf{a}^{\mathrm{H}}\right)^{\mathrm{H}}\mathbf{v} = \left(\mathbf{a}^{\mathrm{H}}\mathbf{v}\right)\mathbf{a} \neq \mathbf{0}. \tag{3.28}$$

It does not remove the ventricular signal component as expected. It does not use any information on that component after all. The MVDR expression from Eq. (3.23) is composed using the $\mathbf{R}_{\mathbf{V+N}}$ and will therefore be able to suppress the ventricular signal component more effectively. This follows from,

$$\mathbf{W}_{\mathrm{MVDR}}^{\mathrm{H}}\mathbf{v} = \frac{\frac{\sigma_n^2}{\sigma_v^2}\left(\mathbf{a}^{\mathrm{H}}\mathbf{v}\right)}{1 + \frac{\sigma_n^2}{\sigma_v^2} - \left(\mathbf{v}^{\mathrm{H}}\mathbf{a}\right)\left(\mathbf{a}^{\mathrm{H}}\mathbf{v}\right)}\mathbf{a} \neq \mathbf{0}. \tag{3.29}$$

It still is not nullified, but the fraction of signal powers should generally be very small, giving a good result. The LCMV should completely remove the ventricular component as prescribed by the constraint in the underlying minimization problem. Using Eq. (3.24) it shows that this is indeed true,

$$\mathbf{W}_{\mathrm{LCMV}}^{\mathrm{H}}\mathbf{v} = \frac{\left(\mathbf{a}^{\mathrm{H}}\mathbf{v}\right)\mathbf{a} - \left(\mathbf{a}^{\mathrm{H}}\mathbf{v}\right)\mathbf{a}}{1 - \left(\mathbf{v}^{\mathrm{H}}\mathbf{a}\right)\left(\mathbf{a}^{\mathrm{H}}\mathbf{v}\right)} = \mathbf{0}. \tag{3.30}$$

3.3.2. Correlation between atrial and ventricular activity

The performance analysis of the aforementioned beamformers shows they very much depend on $\mathbf{a}^{\mathrm{H}}\mathbf{v}$. The Cauchy–Schwarz inequality tells us the following

$$\left|\mathbf{a}^{\mathrm{H}}\mathbf{v}\right| \leq \left|\mathbf{a}^{\mathrm{H}}\mathbf{a}\right|\left|\mathbf{v}^{\mathrm{H}}\mathbf{v}\right| = 1, \tag{3.31}$$

resulting in

$$0 \leq \left|\mathbf{a}^{\mathrm{H}}\mathbf{v}\right| \leq 1. \tag{3.32}$$

Up until now, we have assumed the AA and VA to be very different and uncorrelated. If the atrial and ventricular signal components were fully uncorrelated, this would reflect in their transfer functions as $\mathbf{a}^{\mathrm{H}}\mathbf{v} = 0$. That would actually result in all beamformers working perfectly, if the transfer functions were estimated perfectly.

In reality, there will be a difference in the performance of the beamformers, even if the transfer functions were estimated perfectly. This results from the ATF and VTF actually correlating a little. The performance analysis shows that for all four considered beamformers, the performance degrades with increasing correlation $\mathbf{a}^{\mathrm{H}}\mathbf{v}$. If the correlation would hypothetically saturate as $\left|\mathbf{a}^{\mathrm{H}}\mathbf{v}\right| \to 1$, the beamformers would not be able to distinguish the atrial and ventricular components at all, meaning they would remove both (EBE) or keep both intact (DAS, MVDR, LCMV). In case of the LCMV, it could actually result in a division by zero, making the beamformer unstable.

Realistically, it is almost impossible for the correlation to be maximized, because the AA cannot reach all electrodes at the same time, like the VA does, unless $M = 2$. This, precisely, is the problem with the BE. Rotating the BE will find exactly two orientations in which the atrial propagation wave approaches both unipolar electrodes at the same time. This will maximize the correlation between the ATF and VTF. With increasing M, this should not be a problem anymore.

3.3.3. Trade-off beamformer

Another thing to note, is that the MVDR is actually a trade-off between removing the noise and removing the ventricular signal component depending on the fraction of their signal powers; let us call it α

$$\alpha = \frac{\sigma_n^2}{\sigma_v^2}. \tag{3.33}$$

The expression of MVDR in Eq. (3.23) can even be rewritten into the expressions of the DAS and LCMV beamformers in Eqs. (3.20) and (3.24) respectively for certain values of that α. If the noise power is way bigger than the ventricular signal power, α goes to infinity and the MVDR tends to the DAS expression in Eq. (3.20), removing mostly noise, that is

$$\lim_{\alpha\to\infty} \mathbf{W}_{\mathrm{MVDR}} = \lim_{\alpha\to\infty} \frac{\left(\alpha^{-1}+1\right)\mathbf{a}\mathbf{a}^{\mathrm{H}} - \alpha^{-1}\left(\mathbf{v}^{\mathrm{H}}\mathbf{a}\right)\mathbf{v}\mathbf{a}^{\mathrm{H}}}{\alpha^{-1}+1-\alpha^{-1}\left(\mathbf{v}^{\mathrm{H}}\mathbf{a}\right)\left(\mathbf{a}^{\mathrm{H}}\mathbf{v}\right)} = \mathbf{W}_{\mathrm{DAS}}. \tag{3.34}$$

If the ventricular signal power, however, is bigger than the noise power, α goes to zero and the MVDR tends to the LCMV, that is

$$\lim_{\alpha\to 0} \mathbf{W}_{\mathrm{MVDR}} = \lim_{\alpha\to 0} \frac{(1+\alpha)\,\mathbf{a}\mathbf{a}^{\mathrm{H}} - \left(\mathbf{v}^{\mathrm{H}}\mathbf{a}\right)\mathbf{v}\mathbf{a}^{\mathrm{H}}}{1+\alpha-\left(\mathbf{v}^{\mathrm{H}}\mathbf{a}\right)\left(\mathbf{a}^{\mathrm{H}}\mathbf{v}\right)} = \mathbf{W}_{\mathrm{LCMV}}. \tag{3.35}$$

In general, the noise power is way smaller than the ventricular signal power. This will result in the MVDR resembling the LCMV a lot. They should be able to remove the ventricular component in a good way. The DAS will probably not be very successful, because it focuses on the small noise component.

3.4. Implementation

Before being able to test the beamformer expressions against any data, they must be implemented. The implementation is done in MATLAB and can be found in Appendix A.

The data we start with, consists of M electrode channels, each showing L time samples per K heart beats. All algorithms are implemented per heart beat k, that is, the signal is manually cut into pieces of L samples that include one atrial and ventricular peak. This is done because the cross-correlation matrices and transfer functions are assumed to be stationary per heart beat, but not across multiple heart beats.

Each heart beat is then windowed into K_w pieces of L_w samples using a Hann window with an overlap of 50%. Those windows are zero-padded to L samples and transformed to the Fourier domain using the fast Fourier transform (FFT), thus each consisting of L frequency bins.

The noisy cross-correlation matrix $\mathbf{R}_{\mathbf{X}}$ is defined as

$$\mathbf{R}_{\mathbf{X}} = \mathrm{E}\left[\mathbf{X}\mathbf{X}^{\mathrm{H}}\right], \tag{3.36}$$

but will be estimated per beat k and per frequency bin f as an average over all K_w windows using realization $\mathbf{x}$ of stochast $\mathbf{X}$ as

$$\hat{\mathbf{R}}_{\mathbf{X}}[k,\,f] = \frac{1}{K_w}\sum_{k_w=1}^{K_w} \mathbf{x}[k,\,f,\,k_w]\,\mathbf{x}^{\mathrm{H}}[k,\,f,\,k_w]. \tag{3.37}$$

Using the noisy cross-correlation matrix, we can make an estimate of the VTF $\mathbf{v}$ per beat k. We will only estimate the magnitude part of the transfer function and ignore the phase part, because the changes across the electrodes of the VA are only in magnitude and not in delay. This also means the VTF is the same across all frequency bins f and can be averaged among them to get a better estimate. An eigenvalue decomposition of $\mathbf{R}_{\mathbf{X}}$ is composed per frequency bin f and the eigenvector most resembling an all-ones vector is found using a dot-product,

$$\hat{\mathbf{v}}[k,\,f] = \arg\max_{\mathbf{v}} \left|\mathbf{U}^{\mathrm{H}}[k,\,f]\mathbf{1}\right|, \tag{3.38}$$

where $\mathbf{U}$ is the matrix containing all eigenvectors of $\mathbf{R}_{\mathbf{X}}$, defined per heart beat k and per frequency bin f. The ventricular signal component is not prominently present across all frequency bins, this will result

in some frequency bins without a valid eigenvector. Therefore, a selection is made based on how well the resemblance with the all-ones vector is before averaging across those frequency bins, that is,

$$\hat{\mathbf{v}}[k] = \frac{1}{\beta L} \sum_{f=1}^{\beta L} \hat{\mathbf{v}}[k, f], \tag{3.39}$$

where β is the percentage of frequency bins selected, which is heuristically chosen to be $\beta = 10\%$ in this implementation. The top 10% across all L_w is thus averaged to get an estimate of VTF $\mathbf{v}$ per heart beat k.

The next step is composing the interference cross-correlation matrix $\mathbf{R}_{\mathbf{V+N}}$ using the VTF as

$$\hat{\mathbf{R}}_{\mathbf{V+N}}[k] = \mu \mathbf{v}[k]\mathbf{v}^{\mathrm{H}}[k] + \mathbf{I}, \tag{3.40}$$

where μ is a fraction of the ventricular and noise signal powers and is heuristically set to

$$\mu = \frac{\sigma_v^2}{\sigma_n^2} = 10^5. \tag{3.41}$$

Using the two estimates of cross-correlation matrices it is possible to make an estimate of ATF $\mathbf{a}$ per heart beat k and frequency bin f. With $\mathbf{Q}$ being a matrix containing the sorted left eigenvectors of $\mathbf{R}_{\mathbf{V+N}}^{-1}[k]\mathbf{R}_{\mathbf{X}}[k, f]$ according to their corresponding eigenvalues, we can estimate the ATF as

$$\hat{\mathbf{a}}[k, f] = \mathbf{Q}[k, f]\mathbf{e}_1. \tag{3.42}$$

Now we have all ingredients to actually perform the filtering using the four beamformers per heart beat k, time window k_w and frequency bin f. Afterwards these signals $\mathbf{y} = \mathbf{W}^{\mathrm{H}}\mathbf{x}$ will be transformed back to the time domain using the inverse fast Fourier transform (IFFT) and truncated to size L_w. Then the windows will be combined into one time series using the overlap-and-add technique with once again an overlap of 50%.

3.5. Results

For the results, the proposed atrial estimation method using beamformers DAS, MVDR and LCMV is compared against the beamformer implementation of the bipolar electrode, the EBE. We will do tests with two different estimates of the VTF, several noise levels and different amounts of electrodes. The EGMs, that are filtered, are simulated and thus not true clinical data, as this enables us to compare with the true AA.

3.5.1. Simulated data

The simulated EGMs are composed as described by Sun *et al.*, simulating EGMs with a sampling frequency of $F_s = 1\,\mathrm{kHz}$ of length $T = 5\,\mathrm{s}$ with and without AF [30]. It simulates 5×5 electrodes, thus $M = 25$. The model simulates AF by adding multiple focal sources and by inserting areas of badly conducting tissue. With this simulated data, the AA and VA are separately available, which makes it easy to test the results.

We will consider four different data sets with increasing difficulty in terms of the complexity of the AF. S1 is the simplest case with normal SR, thus without any AF. S2 through S4 all contain AF. S2 and S3 are still rather simple and only contain two focal sources. S4 consists of very complex signals with up to five focal sources. Fig. 3.1 shows an example of one electrode of each data set. Fig. 3.2 shows the complexity levels regarding the differences across the M electrodes.

The VA is the same across all four data sets and approximately the same across the electrodes, which was one of the assumptions the filtering method was based on. Fig. 3.3 shows one beat of the ventricular signal component across all channels m.

The last component of the simulated EGMs is the noise. It will be indicated in terms of a signal-to-noise ratio (SNR) with respect to the atrial signal component.

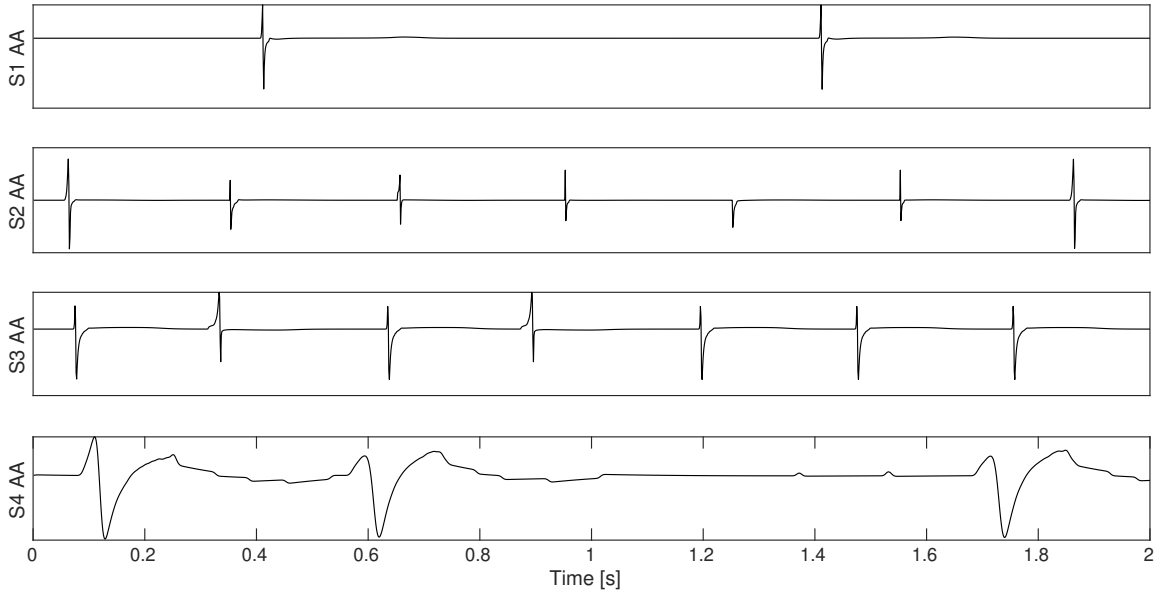

Figure 3.1: A time domain plot of the atrial component in the EGMs. Each subplot shows the first two seconds of the first electrode of each data set S1 through S4, showing the differences in complexity.

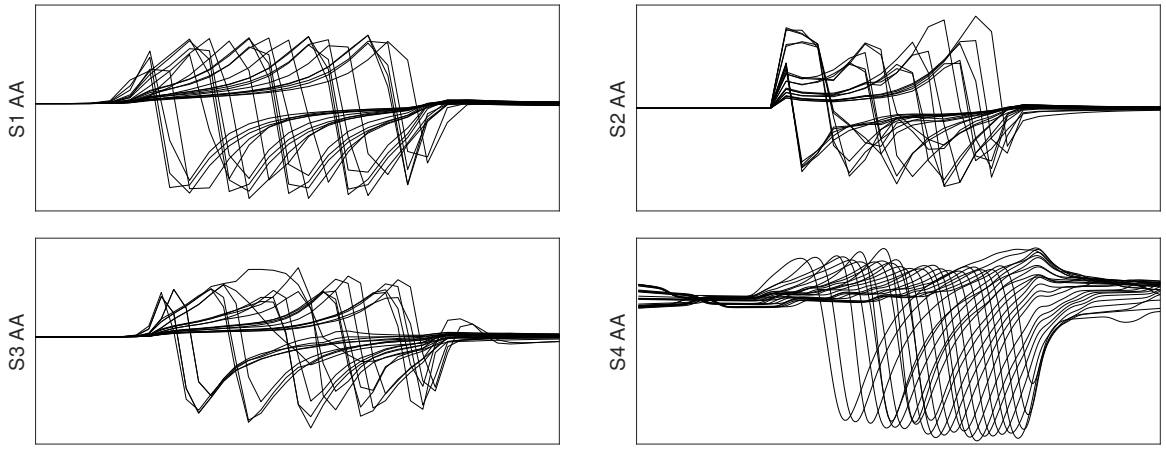

Figure 3.2: A time domain plot of the atrial component in the EGMs. Each subplot shows the same atrial pulse of all electrodes of each data set S1 through S4, demonstrating the differences in complexity.

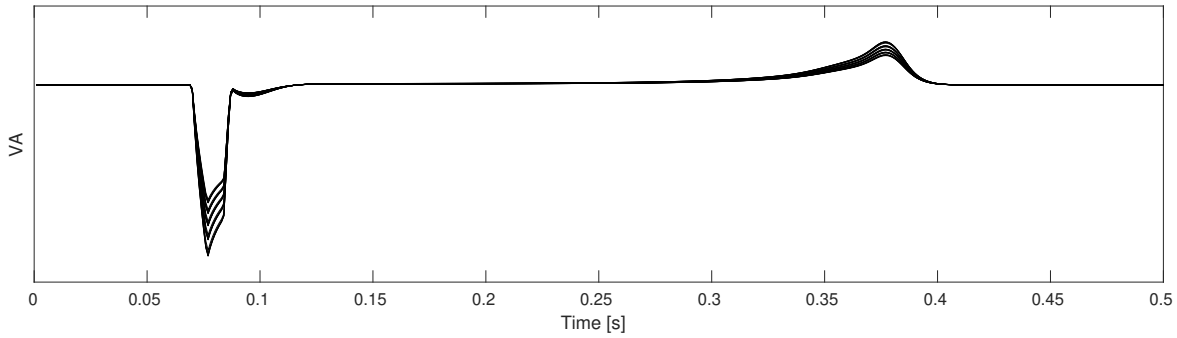

Figure 3.3: A time domain plot of the ventricular component in the EGMs. The plot shows one beat of each electrode.

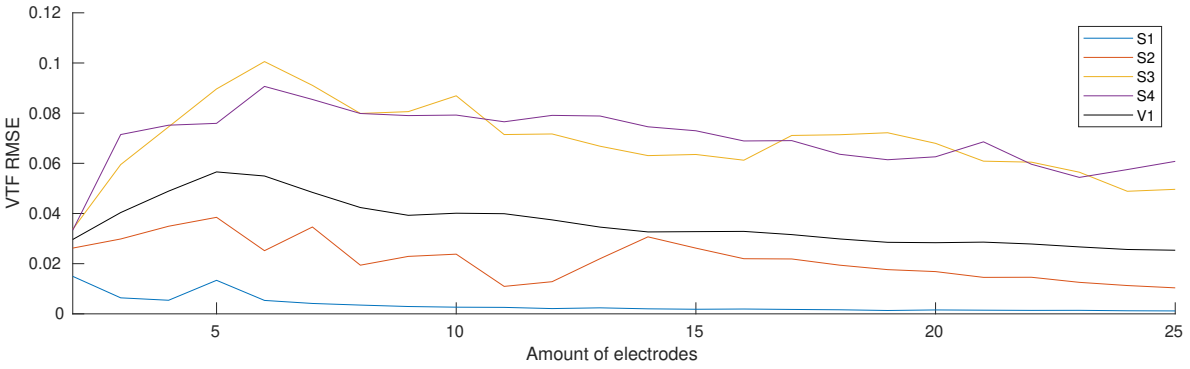

Figure 3.4: A comparison of the eigenvector estimate of the VTF against the all-ones method. The plot shows the RMSE values of V2 for all four data sets, compared against the V1 method for increasing numbers of electrodes M. The V1 method is the same for all sets. The EGMs have been composed with an SNR of $15\,\mathrm{dB}$.

3.5.2. Root-mean-square error

For most results, we will use the root-mean-square error (RMSE). It is a frequently used measure for the difference between an estimator and the true value it tries to estimate. For an estimator $\hat{\boldsymbol{\theta}}$ of value $\boldsymbol{\theta}$ of length N, it is calculated as its name states,

$$\mathrm{RMSE}_\theta = \sqrt{\frac{1}{N}\sum_{n=1}^{N}\left|\hat{\theta}_n - \theta_n\right|^2} = \sqrt{\frac{1}{N}\left(\hat{\boldsymbol{\theta}} - \boldsymbol{\theta}\right)^{\mathrm{H}}\left(\hat{\boldsymbol{\theta}} - \boldsymbol{\theta}\right)}. \tag{3.43}$$

Because we actually have the true AA, it is possible to calculate the atrial and ventricular RMSE. The time-domain atrial signal component should satisfy $\hat{\mathbf{s}}_a = \mathbf{s}_a$, thus the atrial RMSE (ARMSE) can be calculated as

$$\mathrm{ARMSE} = \sqrt{\frac{1}{N}\left(\hat{\mathbf{s}}_a - \mathbf{s}_a\right)^{\mathrm{H}}\left(\hat{\mathbf{s}}_a - \mathbf{s}_a\right)}. \tag{3.44}$$

The time-domain ventricular signal component should be removed, that is $\hat{\mathbf{s}}_v = \mathbf{0}$. The ventricular RMSE (VRMSE) can therefore be calculated as

$$\mathrm{VRMSE} = \sqrt{\frac{1}{N}\hat{\mathbf{s}}_v^{\mathrm{H}}\hat{\mathbf{s}}_v}, \tag{3.45}$$

which essentially is the signal power of the remaining ventricular signal component after filtering.

3.5.3. Ventricular transfer function

One of the first steps in the algorithm is making an estimate of the VTF. We will look at two cases: using the simple all-ones estimate (V1) and using the eigenvector estimate (V2) as proposed in Section 2.2. To get a grasp of how well these estimates, they are compared to a better estimate of VTF from the pure VA.

Fig. 3.4 shows the RMSEs for all four data sets, as well as the V1 estimate which is the same for all data sets for increasing number of electrodes M. For the simpler two sets S1 and S2 the eigenvector method is better than the all-ones method for any M, but it fails to give a good estimate for the more complicated sets S3 and S4.

The true ATF is hard to calculate from the clean AA in a way that gives a better estimate than the method used in this thesis with the noisy cross-correlation matrix. It is therefore not possible or fair to calculate the RMSE of those values.

3.5.4. Bipolar electrode

First, we will look at the simple bipolar electrode to understand why better AA estimation is necessary. The bipolar electrode is the difference between two closely located electrodes. This method, however,

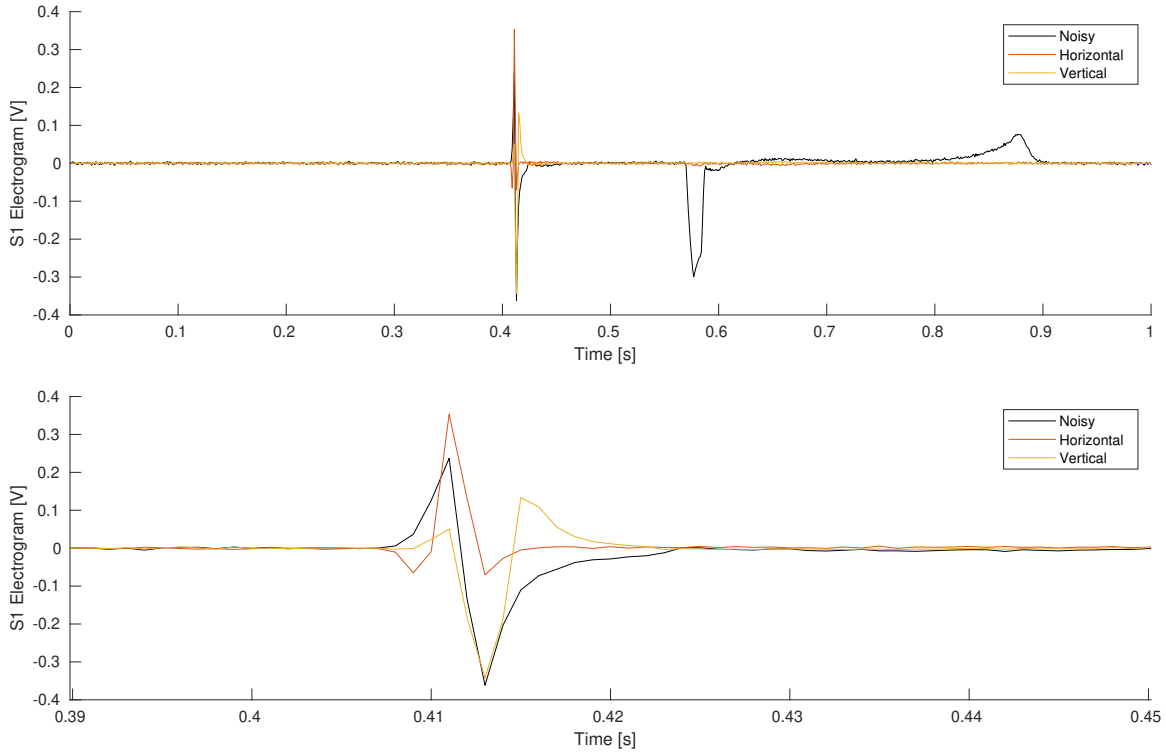

Figure 3.5: A comparison of two different orientations of bipolar electrodes against the noisy EGM of S1, where the bottom plot is a zoomed version of the top one. The EGMs have been composed with an SNR of $20\,\mathrm{dB}$.

very much depends on the orientation of the two electrodes with respect to the atrial signal wave front. Fig. 3.5 shows the difference between two bipolar orientations, horizontal and vertical. The AA is deformed and very different for both orientations as well.

The bipolar electrode is thus able to remove the VA, but the AA is distorted. The more complex beamformers will try to keep the AA intact, but they are not able to remove the VA with only two electrodes, as shown by Fig. 3.6. This means, the amount of electrodes M should be higher.

3.5.5. Sinus rhythm

Using $M = 25$ electrodes instead of just the two gives better results for S1. Fig. 3.7 shows that the EBE has a better estimate of AA using all electrodes instead of just two, but the DAS, MVDR and LCMV have an even better estimate. The DAS is the only one not able to remove the VA effectively.

The amount of electrodes M clearly has an influence on the performance of the beamformers. We can look at a plot where the ARMSE is plotted against the VRMSE for increasing numbers of electrodes M, shown in Fig. 3.8 on a logarithmic scale. Left on the chart means good AA estimation and thus little atrial distortion. Low on the chart means good ventricular suppression. The chart also shows the original ventricular signal power, that the beamformers should be able to diminish.

For this simple data set, the V2 gives the best results. Especially the MVDR and LCMV end up in the lower left corner for high M, which is a good sign. The DAS is not able to remove the VA as effectively, its line almost does not leave the dotted line, meaning it does not remove the VA at all. The EBE has worse atrial estimation than the other beamformers. From the left subplot follows that the beamformers do benefit from a good VTF estimate; V1 gives worse ARMSE and VRMSE. The three complex beamformers stay close to the ventricular dotted line, they are not able to remove that ventricular signal component. The LCMV is cut from the chart for low M, because it had bad performance. Due to the similar AA and VA for low M, it is unstable.

3.5.6. Atrial fibrillation

The eventual goal of the AA estimation is to use it in those cases where the data is less regular than the SR data in S1 and especially data where AA and VA overlap in time. First, we will look at the S2 data in

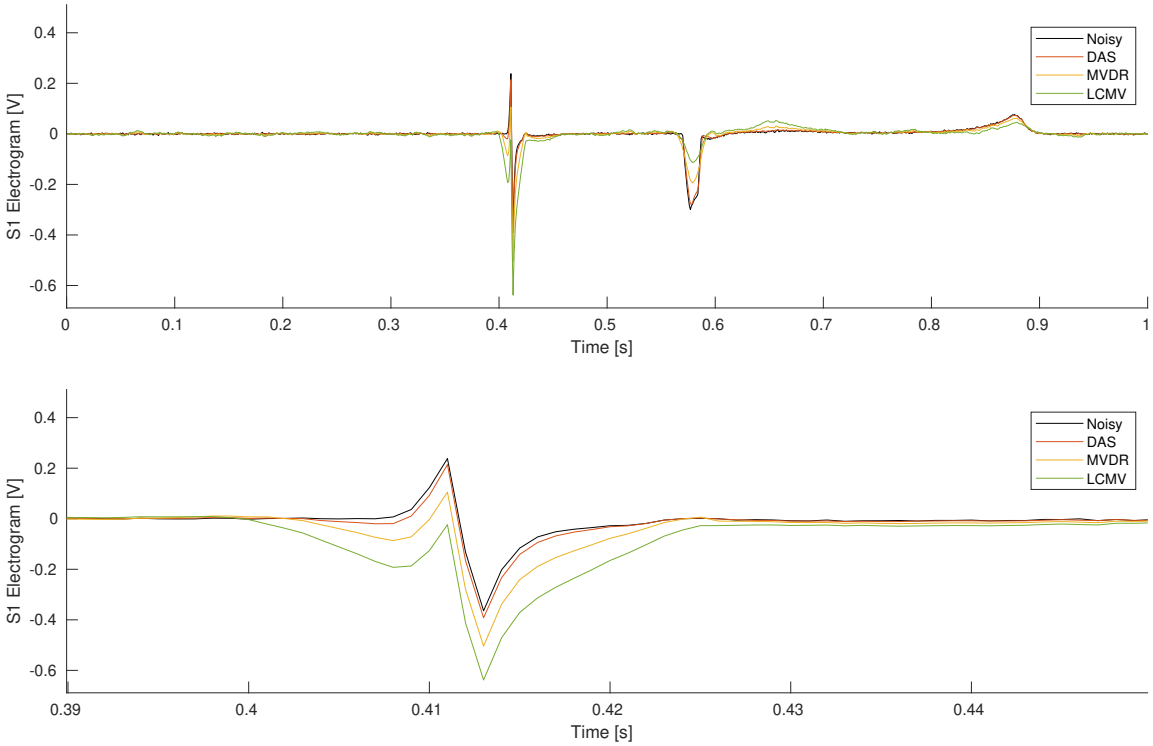

Figure 3.6: A comparison of the three beamformers using all-ones VTF against the noisy EGM of S1 using only two electrodes, where the bottom plot is a zoomed version of the top one. The EGMs have been composed with an SNR of $20\,\mathrm{dB}$.

Fig. 3.9. The MVDR is not visible on the plots, because it overlaps with the LCMV. The MVDR/LCMV is performing better than the DAS and the EBE. From the ARMSE-VRMSE chart in Fig. 3.10 follows that the MVDR and LCMV are best, DAS is worst in terms of ventricular suppression and EBE is worst in terms of atrial distortion. The LCMV is once again unstable for low M.

S3 actually has some overlapping AA and VA. Fig. 3.11 shows two parts of filtered EGMs. The EBE and DAS are again performing worst, but the MVDR and LCMV are also not fully able to remove the VA. Fig. 3.12 shows the ARMSE-VRMSE chart of S3. The DAS clearly performs worst for both V1 and V2. The EBE seems to be performing the best out of the four beamformers. The results of V1 seem to be comparable to those of V2.

S4 is the most irregular data set and is hard to filter effectively, as follows from Fig. 3.13. Most of the VA is removed by the beamformers, but the filtering leaves some artifacts. Furthermore, the AA is affected as well. The artifacts also show up in the ARMSE-VRMSE chart in Fig. 3.14. The complex beamformers give bad results compared to the EBE, which does benefit from the better V2 estimate.

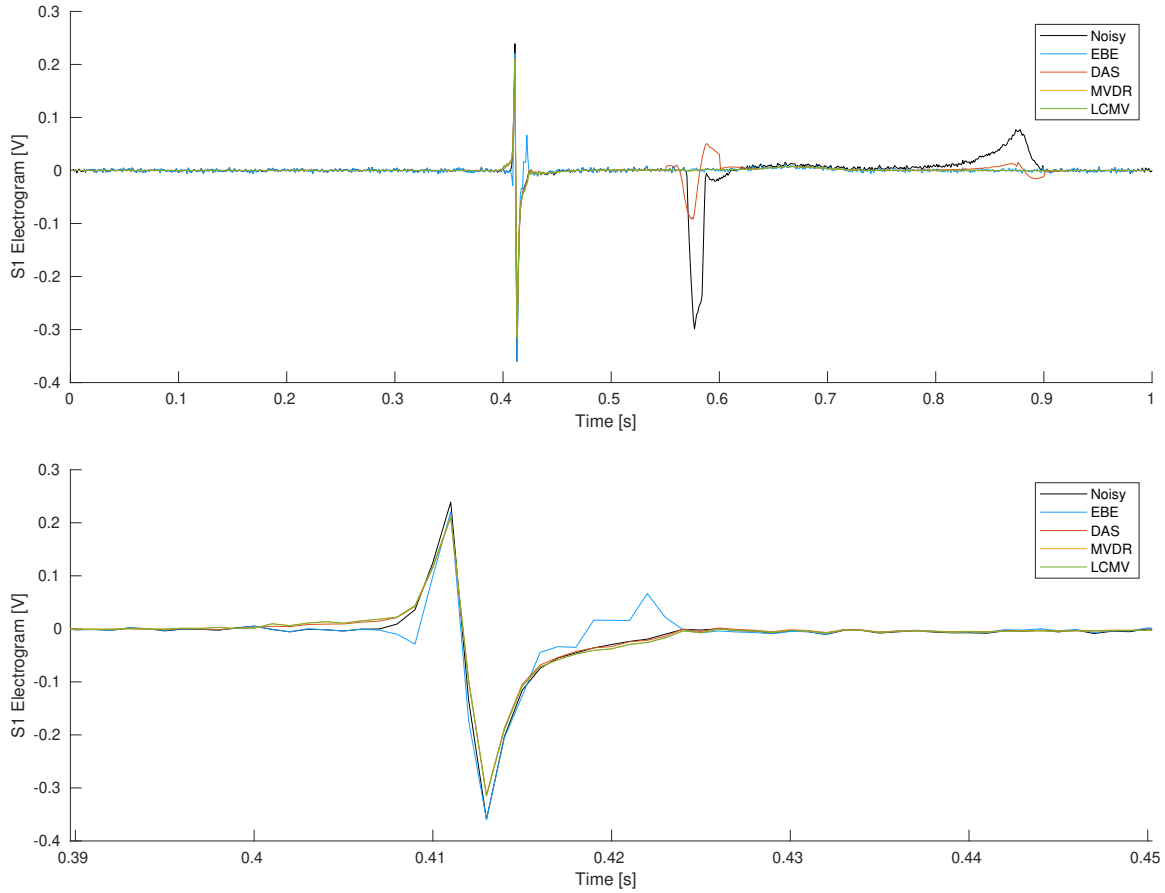

Figure 3.7: A comparison of the four beamformers using V2 against the noisy EGM of S1 using all $M = 25$ electrodes, where the bottom plot is a zoomed version of the top one. The EGMs have been composed with an SNR of $20\,\mathrm{dB}$.

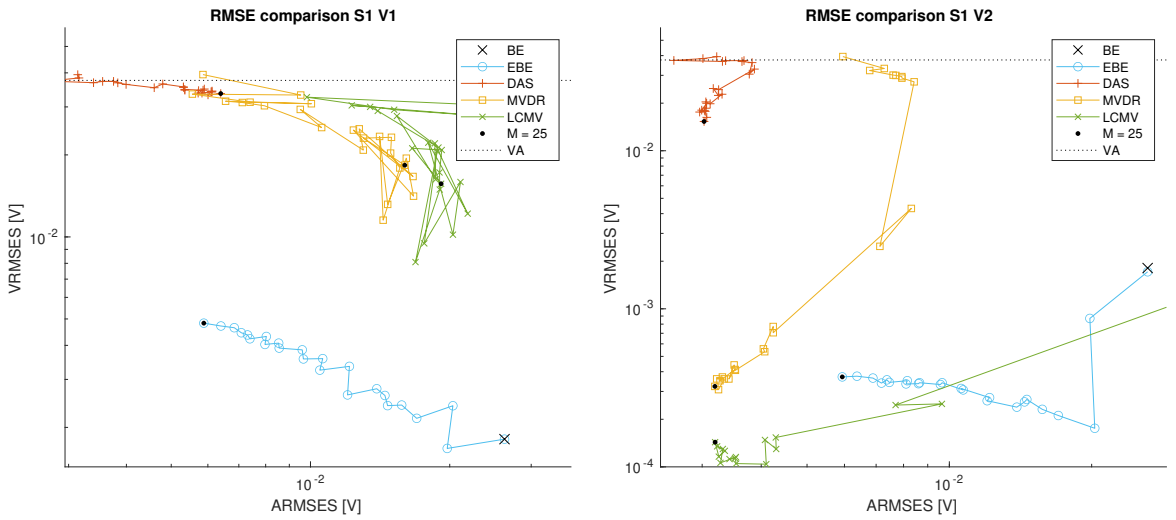

Figure 3.8: A logarithmic chart of the comparison of the ARMSEs and the VRMSEs for all four beamformers of S1 for both V1 and V2 for increasing number of electrodes M. M increases from 2 to 25, where $M = 25$ is indicated with a black dot. The RMSE of the unfiltered ventricular signal is indicated with a dotted line. Part of the LCMV has been cut off. The EGMs have been composed with an SNR of $20\,\mathrm{dB}$.

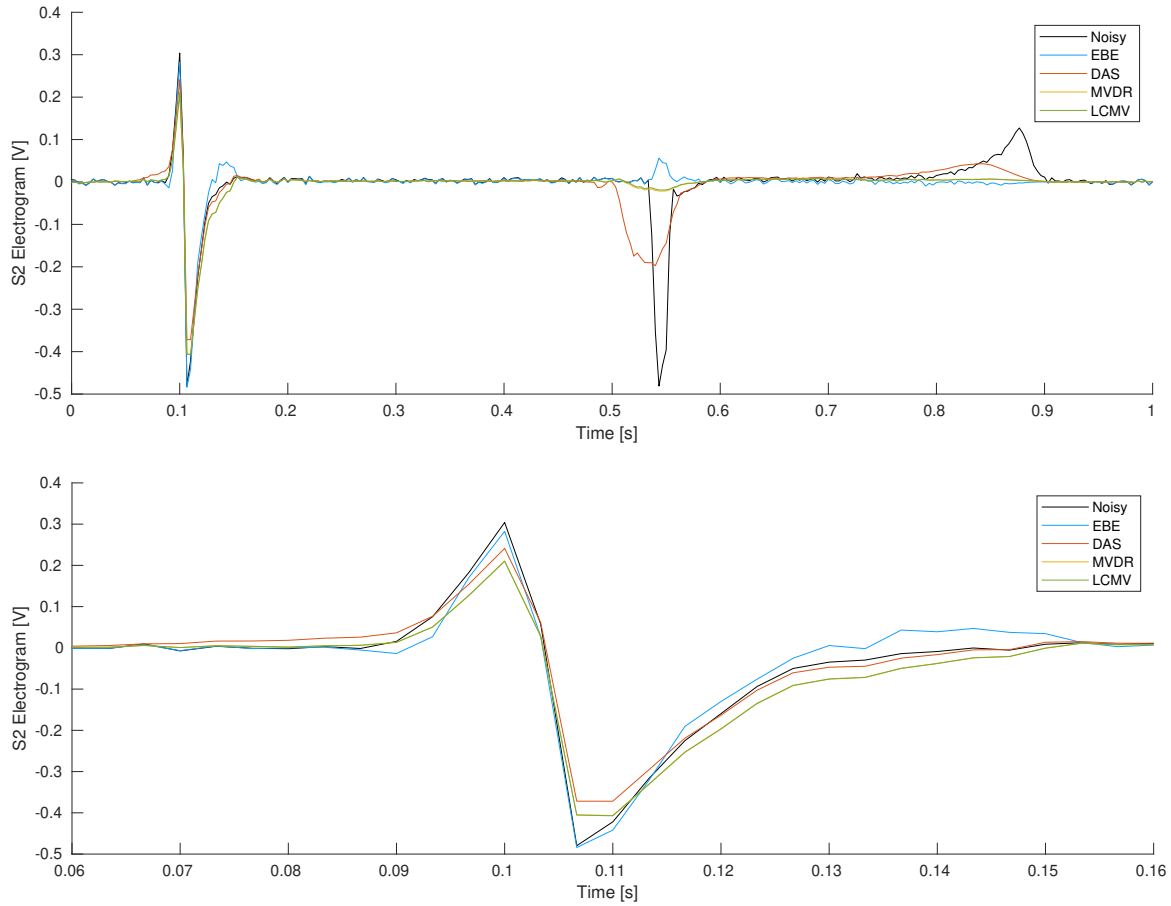

Figure 3.9: A comparison of the four beamformers using V2 against the noisy EGM of S2 using all $M = 25$ electrodes, where the bottom plot is a zoomed version of the top one. The EGMs have been composed with an SNR of $20\,\mathrm{dB}$.

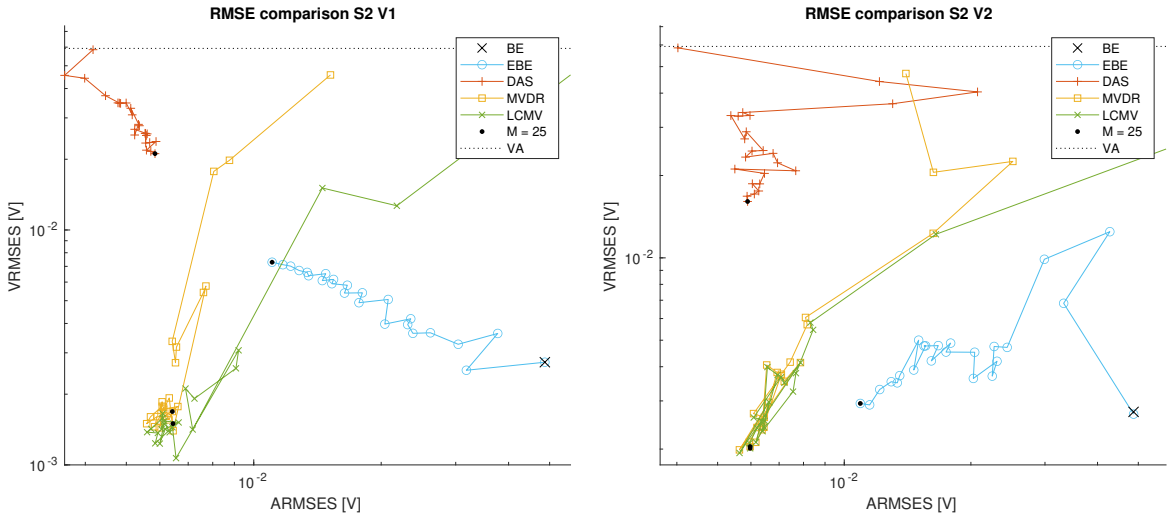

Figure 3.10: A logarithmic chart of the comparison of the ARMSEs and the VRMSEs for all four beamformers of S2 for both V1 and V2 for increasing number of electrodes M. M increases from 2 to 25, where $M = 25$ is indicated with a black dot. The RMSE of the unfiltered ventricular signal is indicated with a dotted line. Part of the LCMV has been cut off. The EGMs have been composed with an SNR of $20\,\mathrm{dB}$.

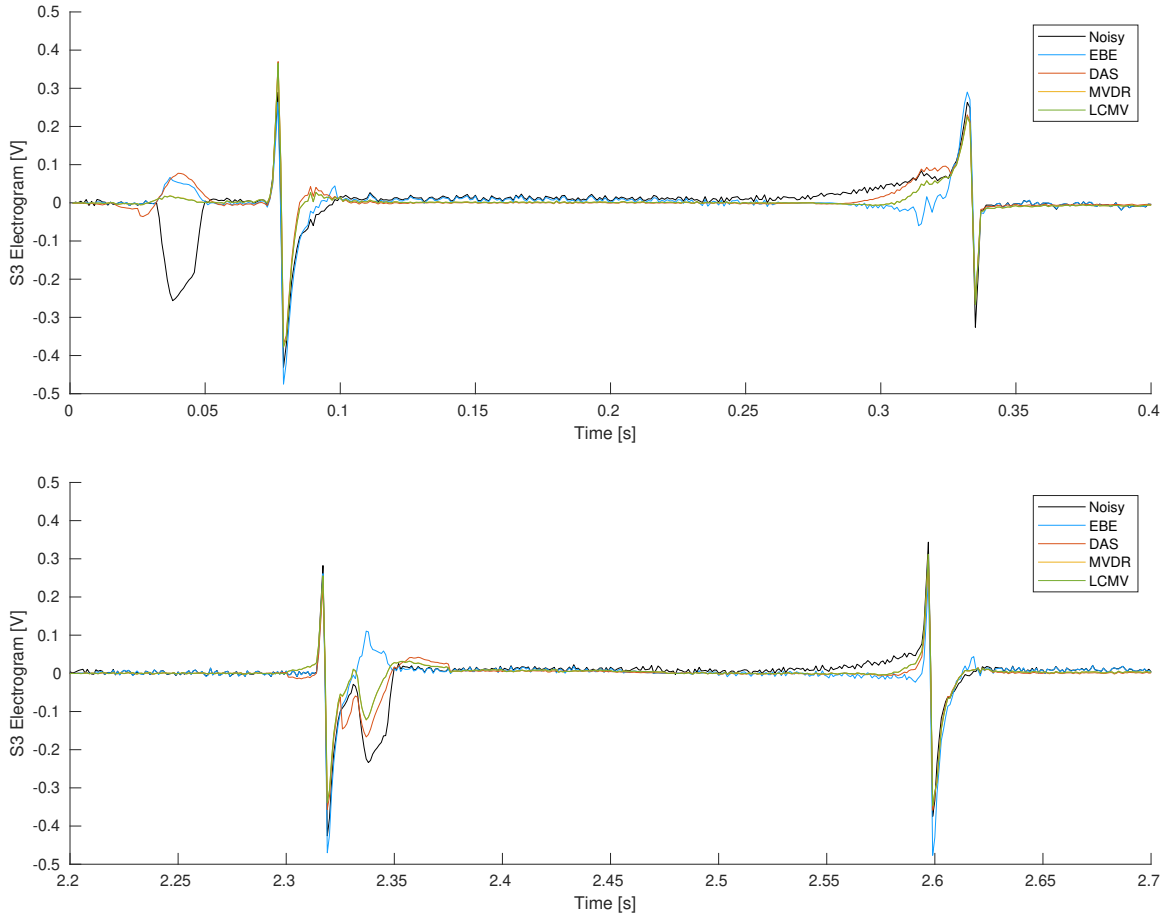

Figure 3.11: A comparison of the four beamformers using V2 against the noisy EGM of S3 using all $M = 25$ electrodes. Both plots show different parts of the full EGM. The EGMs have been composed with an SNR of $20\,\mathrm{dB}$.

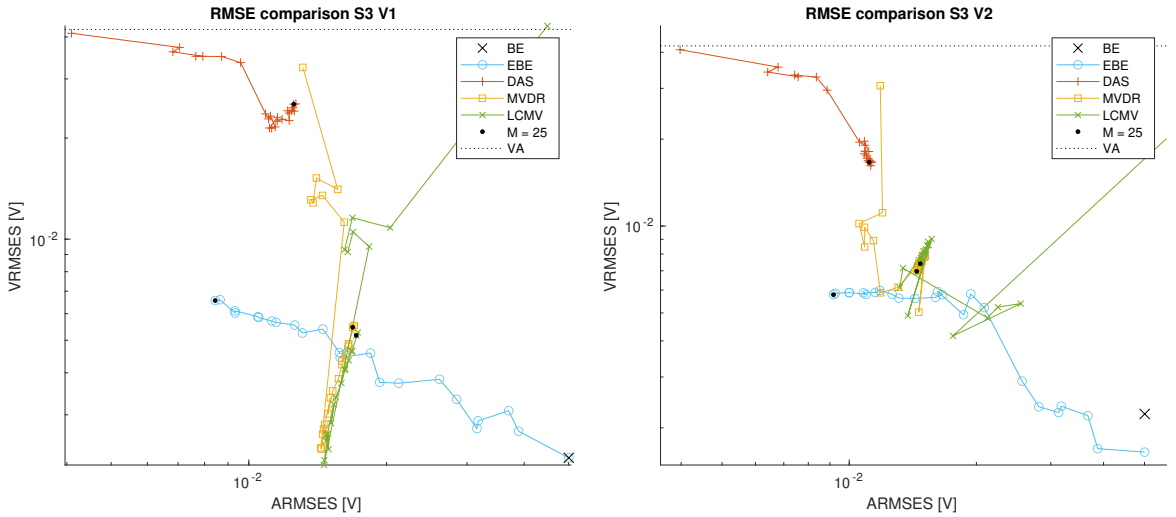

Figure 3.12: A logarithmic chart of the comparison of the ARMSEs and the VRMSEs for all four beamformers of S3 for both V1 and V2 for increasing number of electrodes M. M increases from 2 to 25, where $M = 25$ is indicated with a black dot. The RMSE of the unfiltered ventricular signal is indicated with a dotted line. The BE does not correspond with the start of the EBE line in the right plot, because it does not use V2. Part of the LCMV has been cut off. The EGMs have been composed with an SNR of $20\,\mathrm{dB}$.

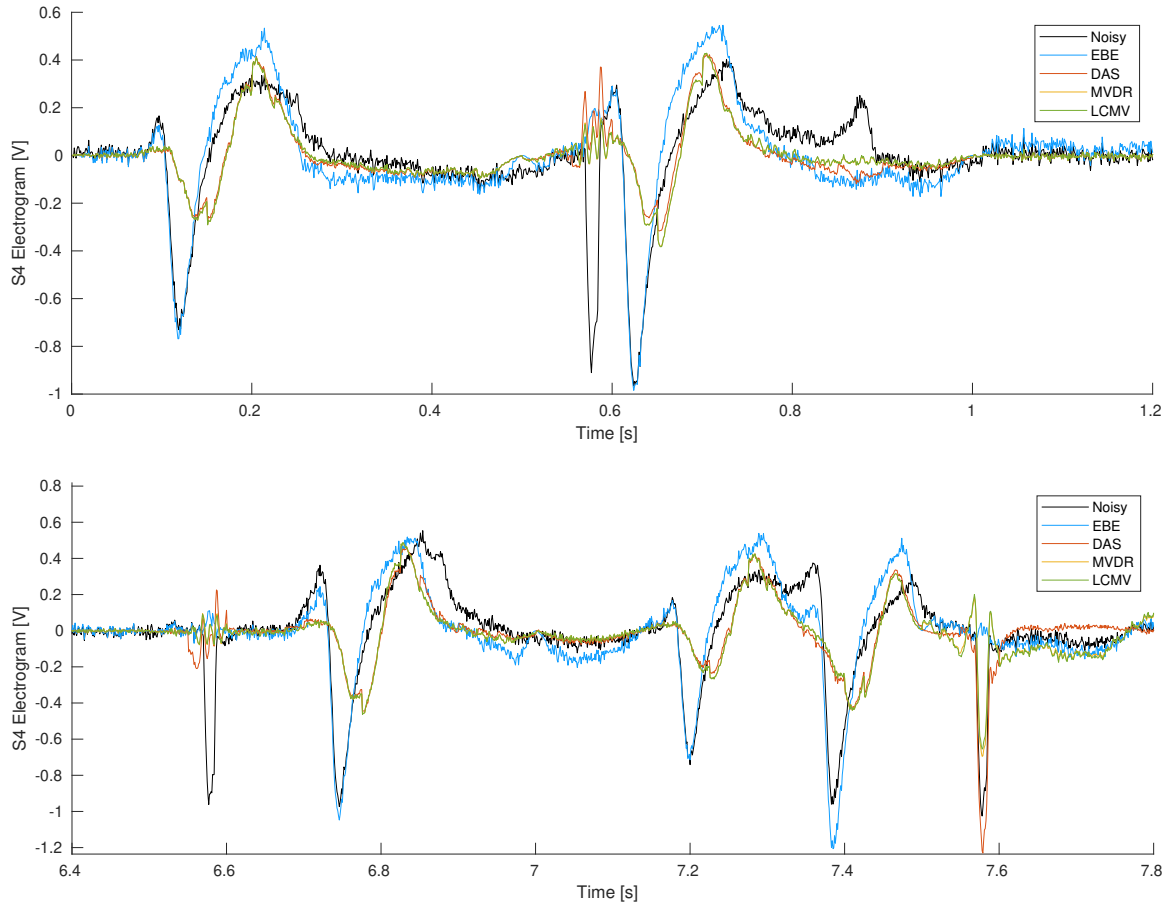

Figure 3.13: A comparison of the four beamformers using V2 against the noisy EGM of S4 using all $M = 25$ electrodes. Both plots show different parts of the full EGM. The EGMs have been composed with an SNR of $20\,\mathrm{dB}$.

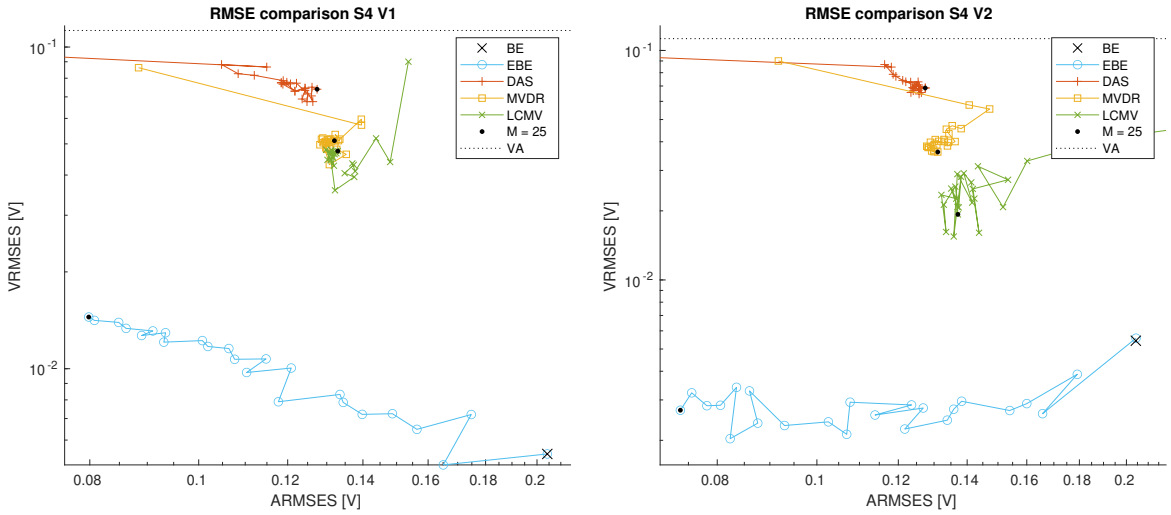

Figure 3.14: A logarithmic chart of the comparison of the ARMSEs and the VRMSEs for all four beamformers of S4 for both V1 and V2 for increasing number of electrodes M. M increases from 2 to 25, where $M = 25$ is indicated with a black dot. The RMSE of the unfiltered ventricular signal is indicated with a dotted line. Part of the LCMV has been cut off. The EGMs have been composed with an SNR of $20\,\mathrm{dB}$.

4

Estimating local activation times

In this chapter the signal model, and especially the ATF, is used to estimate the LATs per heart beat k. These LATs are the moments in time when the tissue underneath the sensors depolarizes, giving a sharp deflection in the measured EGM. Finding these gives insight in the CVs, showing irregularities in the tissue.

In Section 4.1 two example methods from the literature are explained. Section 4.2 explains the proposed method and Section 4.3 the implementation. Section 4.4 then shows the results comparing those to the methods from the literature.

4.1. Literature

Many different methods have been composed to make estimates of the LATs. A LAT is defined as the moment of activation or depolarization of a cell. An electrode will, however, measure multiple cells at once, thus blurring the exact moment as the propagating activation wave will not activate all underlying cells at the same time. The LAT is therefore not trivial.

The LATs can be estimated by physiologists manually, but this is subjective to interpretation and time-invasive. Therefore, multiple automated techniques have been composed [31]. Below are the two main examples.

4.1.1. Steepest deflection

One way to determine LATs, is to look at the steepest deflection (SD) of EGMs [32]. In the sampled EGM data, this comes down to finding the most negative difference between consecutive samples and using the corresponding moment in time as LAT. The computation is very simple, but the method does have a big drawback. It is very susceptible to spikes due to interfering VA or noise.

4.1.2. Cross-correlation

Another method uses a database of templates which will be matched to the EGMs. A more robust approach is to use the surrounding EGMs as templates and correlate [33]. The cross-correlation (CC) of the EGMs against those of neighboring electrodes assumes the EGMs will be similar except for a time-shift. The correlation will thus be highest when performed with a time-shift of the difference of the LATs of both electrodes.

Using this method, only relative LATs will be produced, but considering the application, this is not a problem. The method proposed in this thesis is similar to this cross-correlation method, but does so in the Fourier domain. This sounds more complex, but can be performed easily during the filtering step proposed earlier in this thesis. The time domain version would need this filtering step as well.

4.2. Method

Using ATFs $\mathbf{a}$ per time frame k it is possible to find relative LATs by transforming those back to the time domain, resulting in the atrial impulse response (AIR). A relative ATF with respect to channel m $\mathbf{a}^{(m)}$

can be composed as

$$\mathbf{a}^{(m)}[f,\, k] = \frac{\mathbf{a}[f,\, k]}{a_m[f,\, k]}. \tag{4.1}$$

Without loss of generality, the channel is chosen to be the first one, resulting in relative ATF $\mathbf{a}^{(1)}$, whose first value then is equal to 1 for each f and k.

Combining all frequency bins f per channel m and transforming those frequency series back to the time domain using the inverse Fourier transform, gives M AIRs $h_m[t,\, k]$ per time frame k with respect to the first channel:

$$h_m[t,\, k] = \mathcal{F}^{-1}\left\{a_m^{(1)}[f,\, k]\right\}, \tag{4.2}$$

where $\mathcal{F}^{-1}\{\cdot\}$ is the inverse Fourier transform operator. Now $h_1[t,\, k]$ is a Dirac delta function $\delta[t]$, due to the fact that $a_1^{(1)}[f,\, k] = 1$ is all ones. If all channels would just be time-delayed and amplified versions of the first channel, they would all be Dirac delta functions, albeit delayed and amplified. The LATs can then be found by looking for the moment in time that maximizes the AIRs

$$\mathrm{LAT}_m[k] = \arg\max_t\, h_m[t,\, k]. \tag{4.3}$$

In reality, there will be other differences between the channels as well, but if they are not too big, the algorithm should give accurate results.

4.3. Implementation

The bulk of the MATLAB implementation has been explained in Section 3.4 already. After composing the ATFs per heart beat k and frequency bin f, they have to be normalized with respect to the first electrode to get relative ATFs. Those relative ATFs are transformed back to the time domain using the IFFT to get AIRs. The LAT estimates are made by grabbing the time index t that maximizes the AIRs per heart beat k and per electrode m. For the first electrode this will be time sample $t = 1$, because it is a delta Dirac pulse.

One difficulty has to be overcome: if an electrode m were to be activated before the first electrode, its LAT would have to be negative. The indices, however, can not be negative and the delta peak will wrap around to the end of the AIR time series, resulting in a very large LAT. This problem is solved by adding half the length of the AIR L and applying the modulo operator with that length L and deducting half of L again, that is,

$$\mathrm{LAT}_m[k] = \left(\hat{\mathrm{LAT}}_m[k] + \frac{L}{2} \mod L\right) - \frac{L}{2}. \tag{4.4}$$

Once again, the estimated LATs are only valid relative to each other. The absolute values are not derived using this algorithm.

4.4. Results

For the tests, we will use data sets S1 and S3 mentioned in Section 3.5.1. Those are the only sets we have the true LATs of. The true values will be compared to the estimated values using the RMSE mentioned in Section 3.5.2, as well as compared to the SD and the CC where the last one uses the EGMs filtered using the EBE beamformer to correlate.

The first beats of S1 and S3 are shown in terms of LATs in Figs. 4.1 and 4.2 respectively. The figures show the true LATs and three estimation methods, where the last one is the proposed AIR one. The estimates only differ from the true values by a little.

Figs. 4.3 and 4.4 show the RMSE of the LATs for the three estimation methods for increasing number of electrodes M. For the simple S1 data set, the proposed AIR method is performing better than the state-of-the-art methods for most values of M. For the more difficult S3 this, however, is not the case.

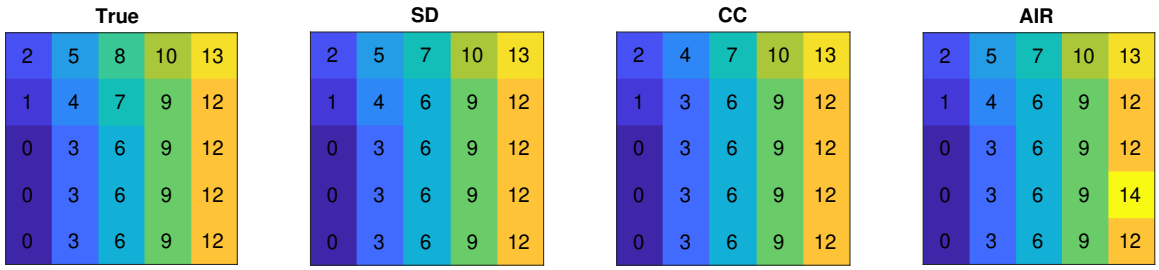

Figure 4.1: True LATs expressed in milliseconds of the first beat of S1 against three estimates of those LATs using the SD, CC and the AIR method proposed in this thesis. The CC and AIR methods use V2. The EGMs have been composed with an SNR of $10\,\mathrm{dB}$.

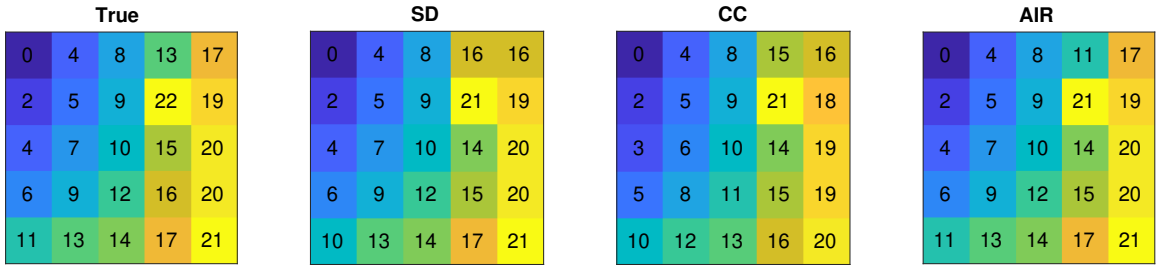

Figure 4.2: True LATs expressed in milliseconds of the first beat of S3 against three estimates of those LATs using the SD, CC and the AIR method proposed in this thesis. The CC and AIR methods use V2. The EGMs have been composed with an SNR of $10\,\mathrm{dB}$.

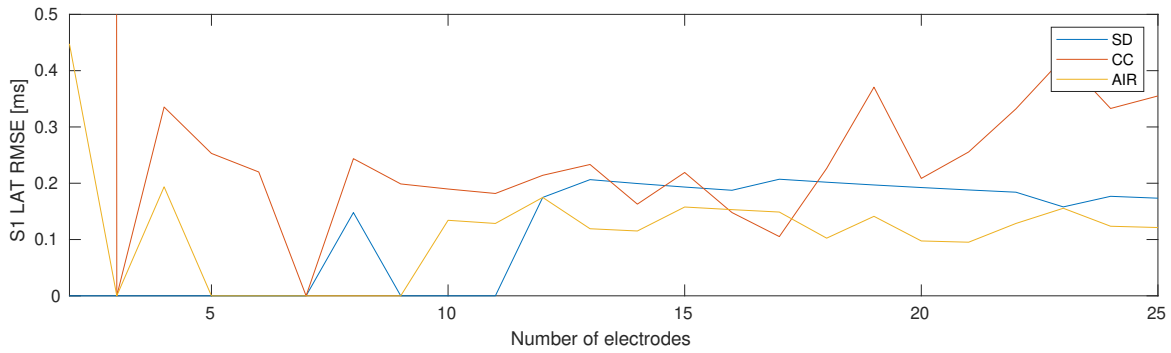

Figure 4.3: The RMSEs of the three estimation methods, SD, CC and AIR, calculated for multiple number of electrodes M in data set S1. The CC and AIR methods use V2. The EGMs have been composed with an SNR of $10\,\mathrm{dB}$.

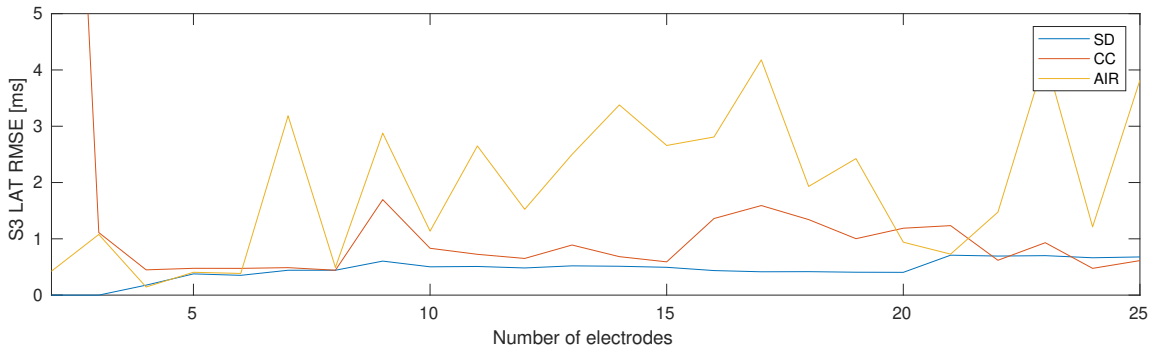

Figure 4.4: The RMSEs of the three estimation methods, SD, CC and AIR, calculated for multiple number of electrodes M in data set S3. The CC and AIR methods use V2. The EGMs have been composed with an SNR of $10\,\mathrm{dB}$.

5

Conclusion and future work

This thesis proposes a new method of estimating the atrial activity (AA) in epicardial electrograms (EGMs) by removing the interfering ventricular activity (VA). This is in particular important when studying atrial fibrillation (AF), where the atrial and ventricular component often overlap. The algorithm for AA estimation uses the spatial information in the multiple electrodes in the Fourier domain. This filtering method is called beamforming, which exploits the underlying spatial transfer functions. These atrial transfer functions (ATFs) can then also be used directly to make an estimate of the local activation times (LATs).

In Chapter 2 a signal model of the EGMs is composed, consisting of AA, VA and noise. The model considers the AA to be the same across the electrodes except for some delays and differing magnitudes; the same holds for the VA. Those differences can be combined into an ATF and a ventricular transfer function (VTF) in the Fourier domain. The chapter also describes a way to estimate those transfer functions using eigenvalue decompositions of the cross-correlation matrices of the EGMs.

In Chapter 3 the signal model and transfer functions are used to build three beamformers that are meant to remove the VA and not distort the AA. The beamformers are also compared to an extended version of the bipolar electrode (BE), which is a simple time-domain average subtraction filter. The three beamformers are compared against the extended bipolar electrode (EBE) in a theoretical sense and in practice by applying them on synthetic data for a range of number of electrodes and scenarios with different degrees of AF.

Chapter 4 uses the ATF to make an estimate of LATs. A LAT is the moment in time when the cells underneath the electrodes are activated and they are used as a visualization technique for physiologists to understand the conduction pattern of the atria. The ATF can be transformed back to the time domain as an atrial impulse response (AIR) from which the peaks should indicate the LATs. The AIR method is compared against two state-of-the-art methods, steepest deflection (SD) and cross-correlation (CC).

5.1. Beamforming

The goal of beamforming in this application is to remove the VA and keep the AA undistorted. Three beamformers are composed with the constraint that the AA remains undistorted if the ATF were estimated perfectly. They are with increasing complexity the delay-and-sum (DAS), the Minimum Variance Distortionless Response (MVDR) and the Linear Constraint Minimum Variance (LCMV) beamformers.

The DAS is not very effective against the VA, while the LCMV mostly focuses on removing the VA, which can make the beamformer unstable for small number of electrodes. The MVDR is a balance between the two and turns out to produce the best results out of the three. The EBE is also placed in the context of beamforming, which from a theoretic perspective shows it does not explicitly keep the AA undistorted.

The beamformers make use of an estimate of the ATF, which is built using two different estimates of the VTF. One is a simple all-ones vector, disregarding any differences in the VA among the electrodes and the other one uses the eigenvalue decomposition of the noisy cross-correlation matrix to make a better estimate of the small magnitudal differences. Both estimates are tested in the beamformers against four data sets with increasing complexity.

The tests on the data sets show that for low numbers of electrodes, the complex beamformers hardly remove any VA, because they cannot do so without distorting the AA, where the EBE does the opposite. When using more electrodes, the results of the four beamformers grow closer in both aspects. For the two simplest data sets, the MVDR and LCMV turn out to be the best choice among the four when using the eigenvector estimate of the VTF. The two have very similar results for large numbers of electrodes. We can say that the MVDR is generally better than the LCMV, because the LCMV is unstable for a low number of electrodes. The DAS is comparable to the MVDR in terms of atrial preservation, but fails to remove the VA effectively. The EBE on the other hand is comparable in terms of ventricular cancellation, but is inferior in terms of the atrial preservation.

When using the simpler all-ones estimate of the VTF, however, the performance of the complex beamformers degrades so much, that the EBE is sometimes better in both atrial preservation and ventricular cancellation. The complex beamformers rely more heavily on a good estimate of that transfer function than the EBE. This does show that the eigenvector estimate is a good addition to the algorithm. The complex beamformers also have difficulties with the two more complicated data sets, which probably is a result of the signal model not being accurate enough for the data. The EBE outperforms the other algorithms for all number of electrodes. The EBE does benefit from the better VTF estimate.

To conclude, it is definitely beneficial to look at more than two electrodes at once when trying to estimate the AA in EGMs. The EBE clearly improves in terms of atrial preservation for increasing numbers of electrodes, albeit sometimes deteriorating a little in terms of ventricular cancellation. The eigenvector estimate for the VTF also has a clear benefit over the simple all-ones estimate. Moreover, the MVDR is able to bring more to the table than the EBE in terms of the atrial preservation, if the signal model is accurate enough for the data set. The MVDR assumes the atrial signal component resembles a lot across the electrodes, meaning there is only one ATF, but this assumption is probably invalid for the more complex data. Furthermore, the LCMV was designed to be better applicable than the MVDR in this atrial problem, but turned out to be somewhat unstable.

5.2. Local activation times

The ATF can also be used to estimate the LATs by normalizing the transfer functions to one electrode and moving it back to the time domain, giving the AIR, whose peaks indicate the LATs. For the simplest data set this works well, outperforming two state-of-the-art methods by a little. The AIR algorithm is, however, not able to give such good results for the harder data set. Once again, this is probably due to the signal model not being accurate enough. The method is therefore not of interest in its current form, because it is a lot more time-consuming as well than the other methods due to the Fourier transforms.

5.3. Future work

The main problem with some of the proposed methods in this thesis is that the underlying signal model is not accurate enough for the more complicated AF data it was meant to process, except for the EBE, which was not derived from the signal model. The model now assumes the atrial signal component is roughly the same across all electrodes, besides some time delay and magnitude differences. From this assumption follows only one ATF and thus a rank-1 atrial cross-correlation matrix. In case of the more complex AF data sets this assumption appears to be invalid.

More research could be done into extending the signal model. One option is to consider a sum of multiple atrial signal and ATF combinations instead of the one $\mathbf{s}_a = s_a\mathbf{a}$, that is,

$$\mathbf{x} = \sum_i s_{a,i}\mathbf{a}_i + s_v\mathbf{v} + \mathbf{n}. \tag{5.1}$$

This would mean that the multiple ATFs have to be estimated and the beamformers have to be extended to using the multiple transfer functions. An alternative is not to use the ATFs, but only to remove the ventricular signal component explicitly, which actually tends towards the EBE again.

Another option is to keep the signal model the same, but to apply it to smaller groups of electrodes. They could be grouped in terms of resemblance by performing some wave front isolation algorithm, under the assumption that the atrial signal component is the same within such a wave front. The signal model would then be valid per group, meaning the algorithm can be applied to those groups.

Furthermore, the algorithm has only been tested with synthetic data. Applying it to clinical data might show other flaws or perks of the algorithm that can be explored.

Bibliography

[1] *The top 10 causes of death*, accessed 18 January 2022, Dec. 2020. [Online]. Available: https://www.who.int/news-room/fact-sheets/detail/the-top-10-causes-of-death.

[2] S. Stewart, C. L. Hart, D. J. Hole, and J. J. V. McMurray, "Population prevalence, incidence, and predictors of atrial fibrillation in the renfrew/paisley study," *Heart*, vol. 86, no. 5, pp. 516–521, Nov. 2001. DOI: 10.1136/heart.86.5.516.

[3] OpenStax College, *Conduction system of heart*, accessed 19 January 2022, Jun. 2013. [Online]. Available: http://cnx.org/content/col11496/1.6/.

[4] G. K. Moe, W. C. Rheinboldt, and J. Abildskov, "A computer model of atrial fibrillation," *American Heart Journal*, vol. 67, no. 2, pp. 200–220, Feb. 1964. DOI: 10.1016/0002-8703(64)90371-0.

[5] M. Haïssaguerre, P. Jaïs, D. C. Shah, *et al.*, "Spontaneous initiation of atrial fibrillation by ectopic beats originating in the pulmonary veins," *New England Journal of Medicine*, vol. 339, no. 10, pp. 659–666, Sep. 1998. DOI: 10.1056/nejm199809033391003.

[6] R. Mandapati, A. Skanes, J. Chen, O. Berenfeld, and J. Jalife, "Stable microreentrant sources as a mechanism of atrial fibrillation in the isolated sheep heart," *Circulation*, vol. 101, no. 2, pp. 194–199, Jan. 2000. DOI: 10.1161/01.cir.101.2.194.

[7] I. Nault, S. Miyazaki, A. Forclaz, *et al.*, "Drugs vs. ablation for the treatment of atrial fibrillation: The evidence supporting catheter ablation," *European Heart Journal*, vol. 31, no. 9, pp. 1046–1054, Mar. 2010. DOI: 10.1093/eurheartj/ehq079.

[8] A. Yaksh, L. J. van der Does, C. Kik, *et al.*, "A novel intra-operative, high-resolution atrial mapping approach," *Journal of Interventional Cardiac Electrophysiology*, vol. 44, no. 3, pp. 221–225, Oct. 2015. DOI: 10.1007/s10840-015-0061-x.

[9] M. Beheshti, K. Magtibay, S. Massé, *et al.*, "Determinants of atrial bipolar voltage: Inter electrode distance and wavefront angle," *Computers in Biology and Medicine*, vol. 102, pp. 449–457, Nov. 2018. DOI: 10.1016/j.compbiomed.2018.07.011.

[10] S. Gaeta, T. D. Bahnson, and C. Henriquez, "Mechanism and magnitude of bipolar electrogram directional sensitivity: Characterizing underlying determinants of bipolar amplitude," *Heart Rhythm*, vol. 17, no. 5, Part A, pp. 777–785, May 2020. DOI: 10.1016/j.hrthm.2019.12.010.

[11] D. C. Deno, R. Balachandran, D. Morgan, F. Ahmad, S. Masse, and K. Nanthakumar, "Orientation-independent catheter-based characterization of myocardial activation," *IEEE Transactions on Biomedical Engineering*, vol. 64, no. 5, pp. 1067–1077, May 2017. DOI: 10.1109/tbme.2016.2589158.

[12] S. Saha, D. Linz, P. Sanders, and M. Baumert, "Beamforming-inspired spatial filtering technique for intracardiac electrograms," in *2019 41st Annual International Conference of the IEEE Engineering in Medicine and Biology Society (EMBC)*, IEEE, 2019. DOI: 10.1109/embc.2019.8857194.

[13] S. K. Haldar, K. Magtibay, A. Porta-Sanchez, *et al.*, "Resolving bipolar electrogram voltages during atrial fibrillation using omnipolar mapping," *Circulation: Arrhythmia and Electrophysiology*, vol. 10, no. 9, Sep. 2017. DOI: 10.1161/CIRCEP.117.005018.

[14] J. Riccio, A. Alcaine, S. Rocher, P. Laguna, J. Saiz, and J. P. Martinez, "Omnipolar EGM voltage mapping for atrial fibrosis identification evaluated with an electrophysiological model," in *2020 28th European Signal Processing Conference (EUSIPCO)*, IEEE, Dec. 2020. DOI: 10.23919/eusipco47968.2020.9287670.

[15] M. S. Spach, W. T. Miller, P. C. Dolber, J. M. Kootsey, J. R. Sommer, and C. E. Mosher, "The functional role of structural complexities in the propagation of depolarization in the atrium of the dog. cardiac conduction disturbances due to discontinuities of effective axial resistivity.," *Circulation Research*, vol. 50, no. 2, pp. 175–191, Feb. 1982. DOI: 10.1161/01.res.50.2.175.

[16] A.-J. van der Veen, "Algebraic methods for deterministic blind beamforming," *Proceedings of the IEEE*, vol. 86, no. 10, pp. 1987–2008, 1998. DOI: 10.1109/5.720249.

[17] S.-E. Kotti, R. Heusdens, and R. C. Hendriks, "Clock-offset and microphone gain mismatch invariant beamforming," IEEE, Jan. 2021. DOI: 10.23919/eusipco47968.2020.9287852.

[18] S. Markovich-Golan and S. Gannot, "Performance analysis of the covariance subtraction method for relative transfer function estimation and comparison to the covariance whitening method," in *2015 IEEE International Conference on Acoustics, Speech and Signal Processing (ICASSP)*, IEEE, Apr. 2015. DOI: 10.1109/icassp.2015.7178028.

[19] S. Shkurovich, A. Sahakian, and S. Swiryn, "Detection of atrial activity from high-voltage leads of implantable ventricular defibrillators using a cancellation technique," *IEEE Transactions on Biomedical Engineering*, vol. 45, no. 2, pp. 229–234, 1998. DOI: 10.1109/10.661270.

[20] A. Bollmann, N. Kanuru, K. McTeague, P. Walter, D. DeLurgio, and J. Langberg, "Frequency analysis of human atrial fibrillation using the surface electrocardiogram and its response to ibutilide," *The American Journal of Cardiology*, vol. 81, no. 12, pp. 1439–1445, Jun. 1998. DOI: 10.1016/s0002-9149(98)00210-0.

[21] S. Petrutiu, J. Ng, G. Nijm, H. Al-Angari, S. Swiryn, and A. Sahakian, "Atrial fibrillation and waveform characterization," *IEEE Engineering in Medicine and Biology Magazine*, vol. 25, no. 6, pp. 24–30, Nov. 2006. DOI: 10.1109/emb-m.2006.250505.

[22] J. J. Rieta, V. Zarzoso, J. Millet-Roig, R. Garcia-Civera, and R. Ruiz-Granell, "Atrial activity extraction based on blind source separation as an alternative to QRST cancellation for atrial fibrillation analysis," Sep. 2000. DOI: 10.1109/cic.2000.898457.

[23] J. J. Rieta, F. Castells, C. Sanchez, V. Zarzoso, and J. Millet, "Atrial activity extraction for atrial fibrillation analysis using blind source separation," *IEEE Transactions on Biomedical Engineering*, vol. 51, no. 7, pp. 1176–1186, Jul. 2004. DOI: 10.1109/tbme.2004.827272.

[24] P. Langley, J. Bourke, and A. Murray, "Frequency analysis of atrial fibrillation," in *Computers in Cardiology 2000. Vol.27 (Cat. 00CH37163)*, IEEE, Sep. 2000. DOI: 10.1109/cic.2000.898456.

[25] B. van Veen and K. Buckley, "Beamforming: A versatile approach to spatial filtering," *IEEE ASSP Magazine*, vol. 5, no. 2, pp. 4–24, Apr. 1988. DOI: 10.1109/53.665.

[26] V. Perrot, M. Polichetti, F. Varray, and D. Garcia, "So you think you can DAS? a viewpoint on delay-and-sum beamforming," *Ultrasonics*, vol. 111, p. 106 309, Mar. 2021. DOI: 10.1016/j.ultras.2020.106309.

[27] E. Habets, J. Benesty, I. Cohen, S. Gannot, and J. Dmochowski, "New insights into the MVDR beamformer in room acoustics," *IEEE Transactions on Audio, Speech, and Language Processing*, vol. 18, no. 1, pp. 158–170, Jan. 2010. DOI: 10.1109/tasl.2009.2024731.

[28] G. W. Elko, "Microphone array systems for hands-free telecommunication," *Speech Communication*, vol. 20, no. 3-4, pp. 229–240, Dec. 1996. DOI: 10.1016/s0167-6393(96)00057-x.

[29] J. Sherman and W. J. Morrison, "Adjustment of an inverse matrix corresponding to a change in one element of a given matrix," *The Annals of Mathematical Statistics*, vol. 21, no. 1, pp. 124–127, Mar. 1950. DOI: 10.1214/aoms/1177729893.

[30] M. Sun, N. M. de Groot, and R. C. Hendriks, "Joint cardiac tissue conductivity and activation time estimation using confirmatory factor analysis," *Computers in Biology and Medicine*, vol. 144, p. 105 393, May 2022. DOI: 10.1016/j.compbiomed.2022.105393.

[31] C. Cantwell, C. Roney, F. Ng, J. Siggers, S. Sherwin, and N. Peters, "Techniques for automated local activation time annotation and conduction velocity estimation in cardiac mapping," *Computers in Biology and Medicine*, vol. 65, pp. 229–242, Oct. 2015. DOI: 10.1016/j.compbiomed.2015.04.027.

[32] B. M. Steinhaus, “Estimating cardiac transmembrane activation and recovery times from unipolar and bipolar extracellular electrograms: A simulation study.,” *Circulation Research*, vol. 64, no. 3, pp. 449–462, Mar. 1989. DOI: 10.1161/01.res.64.3.449.

[33] J. Duchateau, M. Potse, and R. Dubois, “Spatially coherent activation maps for electrocardiographic imaging,” *IEEE Transactions on Biomedical Engineering*, vol. 64, no. 5, pp. 1149–1156, May 2017. DOI: 10.1109/tbme.2016.2593003.

A

Matlab code

The MATLAB code below filters the EGMs composed from the atrial and ventricular data inside a mat-file using the four beamformers and shows one of the beats. It furthermore estimates the LATs.

```
%% Compose data
% Receive simulated data from .mat files and add noise
% Data consists of K beats of length L in M channels

load sinusrhythm.mat;

X = awgn(S_a, 10, 'measured') + S_v;
[M, L, K] = size(X);

%% Window data
% Window data per beat k into smaller parts kw of size Lw using a Hann
% window with length L due to zero-padding

Lw = 50;
Sw = floor(Lw / 2);
Kw = floor((L - Sw) / Sw);

Xfw = zeros(M, Kw, L, K);
for k = 1 : K
    x = X(:, :, k)';
    xw = reshape(x((1 : Lw * Kw) - (Lw - Sw) * ...
        kron((1 : Kw) - 1, ones(1, Lw)), :), Lw, Kw, M);
    Xfw(:, :, :, k) = permute(fft(xw .* hanning(Lw), L), [3 2 1]);
end

%% Correlate data
% Build the noisy cross-correlation matrix by averaging over all windows
% kw per beat k

Rxx = zeros(M, M, L, K);
for k = 1 : K
    for l = 1 : L
        Xf = Xfw(:, :, l, k);

        Rxx(:, :, l, k) = Xf * Xf' / Kw;
    end
end

%% Estimate ventricular transfer function
% Estimate the VTF per beat k by looking for the eigenvector closest to
% the all-ones vector and averaging over all frequency bins l

vhat = ones(M, 1) / sqrt(M);

VTF = zeros(M, K);
for k = 1 : K
```

```
    vs = zeros(M, L);
    vm = zeros(1, L);

    for l = 1 : L
        [V, ~] = eig(Rxx(:, :, l, k));

        [vm(l), ind] = max(V' * vhat);
        vs(:, l) = abs(V(:, ind));
    end

    [vm, ind] = sort(vm, 'descend');
    vs = vs(:, ind);

    VTF(:, k) = mean(vs(:, 1 : ceil(0.1 * Lw)), 2);
end

%% Compose interference cross-correlation matrix
% Build the interference cross-correlation matrix using the composed VTF

Rvv = zeros(M, M, K);
Rnn = eye(M);
Rii = zeros(M, M, K);
for k = 1 : K
    v = VTF(:, k);

    Rvv(:, :, k) = v * v';

    Rii = Rvv * 1e2 + Rnn;
end

%% Estimate atrial transfer function
% Estimate the ATF per beat k and per frequency bin l using the GEVD of
% the noisy and interference cross-correlation matrices

ATF = zeros(M, L, K);
for k = 1 : K
    rii = Rii(:, :, k);

    for l = 1 : L
        rxx = Rxx(:, :, l, k);

        [~, d, Q] = eig(rii \ rxx, 'vector');
        [d, ind] = sort(d, 'descend');
        Q = Q(:, ind);

        ATF(:, l, k) = Q(:, 1);
    end
end

%% Filter
% Use beamformers to filter the noisy signals using several different
% beamformer expressions that use the ATF, VTF and interference
% cross-correlation matrix

ps = {'BE', 'DAS', 'MVDR', 'LCMV'};
P = length(ps);

Yfw = zeros(M, Kw, L, P, K);
for k = 1 : K
    v = VTF(:, k);
    rii = Rii(:, :, k);

    for l = 1 : L
        a = ATF(:, l, k);

        for kw = 1 : Kw
            xf = Xfw(:, kw, l, k);

            Yfw(:, kw, l, 1, k) = (eye(M) - v * v')' * xf;
            Yfw(:, kw, l, 2, k) = (a * a')' * xf;
            Yfw(:, kw, l, 3, k) = (rii \ a * a' / (a' / rii * a))' * xf;
```

```
            Yfw(:, kw, l, 4, k) = ((a * a' - v' * a * v * a') / ...
                (1 - v' * (a * a') * v))' * xf;
        end
    end
end

%% Dewindow data
% Move back to the time domain and overlap-and-add the windows into time
% series per beat k after cutting the windows back to size Lw

Y = zeros(M, L, K, P);
for k = 1 : K
    for p = 1 : P
        yfw = ifft(permute(Yfw(:, :, :, p, k), [3 2 1]));

        y = zeros(Lw + (Kw - 1) * Sw, M);
        for kw = 1 : Kw
            ind = (1 : Lw) + (kw - 1) * Sw;

            y(ind, :) = y(ind, :) + squeeze(yfw(1 : Lw, kw, :));
        end

        Y(:, :, k, p) = y';
    end
end

%% Combine all beats
% Combine the signals separated per beat k together

x = reshape(X, [M, L * K]);
s_a = reshape(S_a, [M, L * K]);
t = (1 : (K * L)) / Fs;

y = reshape(Y, [M, L * K, P]);

%% Calculate atrial RMSEs
% Calculate the RMSE of the filtered signals compared to the pure atrial
% signal

MSE_atrial = sqrt(squeeze(mean(mean((y - s_a) .^ 2, 1), 2)))

%% Calculate atrial impulse response
% Calculate the atrial impulse response by dividing the ATF by the entry
% corresponding to its first electrode

H = ifft(ATF ./ ATF(1, :, :), [], 2);

%% Determine local activation times
% The LATs can be determined by looking for the largest values of the
% atrial impulse response and selecting that time sample

[~, Lat_hat] = max(permute(H, [1 3 2]), [], 3);
Lat_hat = mod(Lat_hat + L / 2, L) - L / 2;

%% Calculate LAT RMSEs
% Calculate the RMSE of the LAT calculation

MSE_lats = sqrt(mean(((Lat_hat - min(Lat_hat) + min(Lat)) - Lat) ...
    .^ 2, 'all')) / Fs

%% Plot data for one electrode

plot(t, s_a(1, :), 'DisplayName', 'Atrial');
hold on;
plot(t, x(1, :), 'DisplayName', 'Noisy');
for p = [1 2 3 4]
    plot(t, y(m, :, p), 'DisplayName', ps{p});
end
legend;
xlabel('Time [s]');
ylabel('Electrogram [V]');
```